Norwegian University of Life Sciences

Master's Thesis 2017 30 Credits

Norwegian University of Life Sciences
Faculty of Environmental Science & Technology
Dept. of Mathematical Sciences & Technology

Contribution of Hydrological Mass Variations to Time Series of Absolute Gravimetry

Hydrologiske tidsvariasjoner fra massebidrag til absolutt gravimetri

Bård Hauan Andersen
Geomatics Engineering

Norwegian University of Life Sciences

Faculty of Environmental Science and Technology

Department of Mathematical Sciences and Technology (IMT)

Contribution of hydrological mass variations to time series of absolute gravimetry

Author:
Bård Hauan Andersen

Supervisors:
Dr.-Ing Christian Gerlach
Prof. Jon Glenn Gjevestad

May 12, 2017

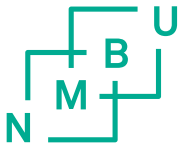

Norwegian University of Life Sciences

Abstract

The gravitational field of the Earth consists of different geophysical elements, which affect how large the absolute gravity value are at different observation sites around the Earth.

This thesis investigates and analyses how the hydrological cycle affects the gravity field over time, when taking into account the gravity attraction correction and the surface loading correction near the surface of the Earth. The thesis covers the variations in gravity given by the hydrological models from the beginning of 2014 to the end of 2016. The global hydrological models have an average correction of $\pm$ 2 μGal, where 60% is caused by the gravity loading correction and 40% by the gravity attraction correction. The seasonal variations in gravity when analysing the global hydrological models are similar to aechother taking into consideration gravity variations, even though there are differences in hydrological inputs and outputs parameters. According to analyses of Global hydrological models, seasonal variations of the models are quite similar when considering the gravity correction, even though the input and output parameters vary.

The local hydrological model is used to calculate the gravity variation correction of the groundwater content close to the observation stations. The model has a maximum variation of 10 μGal at Trysil from peak-to-peak, since the groundwater table is fluctuating during the three years calculated for.

Sammendrag

Jordas gravitasjonsfelt består av flere forskjellige geofysiske elementer, som har påvirkning på hvor stor den absolutte tyngden er på forskjellige steder på jorda.

Denne oppgaven undersøker og analyserer hvordan den hydrologiske syklusen påvirker tyngdefeltet over tid, både med tanke på gravitasjonskraften fra de hydrologiske elementene og deres påvirkning på jordskorpedeformasjoner pga. belastningsfenomener på jordas overflate. Oppgaven dekker variasjoner i de hydrologiske modellene fra 2014 til 2016. De globale hydrologiske modellene har en gjennomsnittskorreksjon på $\pm$ 2 μGal, hvor 65% er forårsaket av jorskorpedeformasjoner og 35% av gravitasjonskraften. Ved analyse av de forskjellige globale hydrologiske modellene vises det at de gir svært like sesongvariasjoner i tyngden, selv om de har forskjellige hydrologiske inn-, og utdata.

I den lokale hydrologiske modellen er grunnvannstanden brukt for å kalkulere tyngdevariasjonseffekten til grunnvannet. Modellen har en variasjon på 10 μGal fra topp til bunn pga. grunnvannsspeilet varierer i løpet av treårsperioden.

Acknowledgement

This thesis marks the end of my work during these 4 months and the end of my student life here in Ås.

I am grateful to "The master programme in Geomatics" for granting me the opportunity to explore this fascinating topic, and my supervisor Christian Gerlach for his expert advise and supportive and inspiring way to give constructive criticism throughout this project. I would also like to thank Jon Glenn Omholdt Gjevestad for explaining geodesy in an easy way during my years here at the Norwegian University of Life Sciences.

Moreover, I will thank my fellow students at the "Geomatics room" for their friendship, especially Eirik Aabøe who helped me with GIS problems. Additionally, I will thank my friend Thomas Ruud for his advice.

Finally, I would like to thank my dear Alise and my parents for supporting me during these last weeks, especially my father Morten who helped me in the end.

Bård Hauan Andersen

Ås, May 2017

Contents

List of Figures

List of Tables

Chapter 1

Introduction

Geodesy come from the Ancient Greek term *geodaisia*, which means "division of Earth". Geodesy is a part of physics, which handle the Earth. It is the science of measuring and analysing the gravity field, geometric shape and orientation of the Earth. Physical geodesy is a section of geodesy which studies the gravity field of the Earth and its variations.

Without gravity, life would not exist. Gravity is what got masses to merge into planets and stars. It is what keep the Earth circulating the Sun and the Moon circulating the Earth. Gravity holds life together, and if gravity vanished, the atmosphere and water in rivers, lakes and oceans would have faded into space. Gravity is divided into two components, one which is the gravitational effect, and the second is the centrifugal acceleration. Gravitation make masses attract each other and centrifugal acceleration is acceleration outwards from the rotational axis.

1.1 Motivation

Changes in mass distribution on the continents of the Earth cause variations in gravity. Analysing the influence of the hydrological cycle and climate changes on gravity is intriguing. The aspects of gravity I will examine are the hydrological gravity attraction and loading correction. The loading correction is caused by water storage changes, which deform and press down the topography. Geodetic observations on the surface of the Earth and mathematical models can be combined to make us understand geophysical signals and systems better. Gravity is closely related to the geoid. Gravity is the gradient of gravity potential and is orthogonal to equipotential surfaces. Gravity is a measure for the distance between equipotential surfaces. The equipotential surface that is situated at mean sea level can be called the geoid.

1.2 Thesis objective

The thesis intention is to investigate the impact of hydrological effects on gravity. Both Global and local models will be analysed and compared to each other.

The main points I will look into are the following:

- How does the global and local gravity attraction effect vary?
- How does the global and local gravity loading effect vary?
- Compare the gravity attraction and loading correction to each other.
- Compare the local and global gravity corrections to absolute gravity data.

I will refer to these four main points in the discussion of the results, and

the analysis of the results make this possible. The theory of the gravity field in the next chapter have been my guiding principles when designing my computations.

The time epoch chosen to analyse the impact of the hydrological models are from the beginning of 2014 to the end of 2016.

1.3 Abbreviations

Abbreviations of the words and phrases in the master thesis is listed here.

GRACE	Gravity Recovery and Climate Experiment
NVE	Norwegian Water Resources and Energy Directorate
LSM	Land surface models
GHM	Global hydrological model
LHM	Local hydrological model
VIC	Variable Infiltration Capacity model
CLM	Community Land Model
NASA	National Aeronautics and Space Administration
GSFC	Goddard Space Flight Center
NCEP	National Centers for Environmental Prediction
NOAA	National Oceanic and Atmosphere Administration
IAU	Incremental Analysis Updates
MERRA	The Modern-Era Retrospective Analysis for Research and Applications
ECMWF	European Centre for Medium-Range Weather Forecast
ERA	ECMWF re-analysis
DEM	Digital elevation model
GIS	Geographical information system
NMBU	Norwegian University of Life Sciences
SG	Superconducting gravimeter

Chapter 2

Theory of the gravity field

2.1 Newton's laws

There are two fields surrounding the earth, one is the electromagnetic field and the other is the gravitational field. In what follows, the components of the gravitational field are defined and clarified. The field I will go into is the gravitational field. The gravitational field exist because of the mass of the earth. The earth has a mass of $5.972 * 10^{24}$ kg. The mass from an object this huge and heavy creates a strong gravitational field which causes a strong attraction on objects several thousand kilometers distance from the earth.

The gravitational theory, which Isac Newton described accurately in the 17th century, states that two particles with masses m_1 and m_2 will enact on each-other with a force F proportional to their mass and the distance r between the center of the masses m_1 and m_2. This means the closer you are to an object, the stronger the pull from that object is.

$$F = G\left(\frac{m_1 m_2}{r^2}\right) \tag{2.1}$$

The mass m_1 causes attraction on the mass m_2 and the mass m_2 does enact the same attraction on m_2, but the opposite way.

While GM is known accurately, G and M is not. The universal constant $G = 6.6740831 * 10^{-11} m^3 kg^{-1} s^{-2}$ is an important empirical physical constant, but not accurate compared to other physical constants [Hoffmann-Wellenhoff et al., 2005].

Let us have a look at the gravitational field around m_1, to make it simpler $m = m_1$

The gravitational attraction g with the unit N/kg or m/s^2 can now be written

$$g = \frac{Gm}{r^2} \tag{2.2}$$

2.2 Vector field and scalar field

The gravitational field g of a particle will consist of vectors directed towards the particle. The further away from the particle, the smaller the length or amplitude of the vector are.

Newtons gravitational law can be written as a vector function with regards to the distance r to points P from the particle m

$$\vec{g}(P) = Gm\frac{\vec{r}}{\vec{r}^3} \tag{2.3}$$

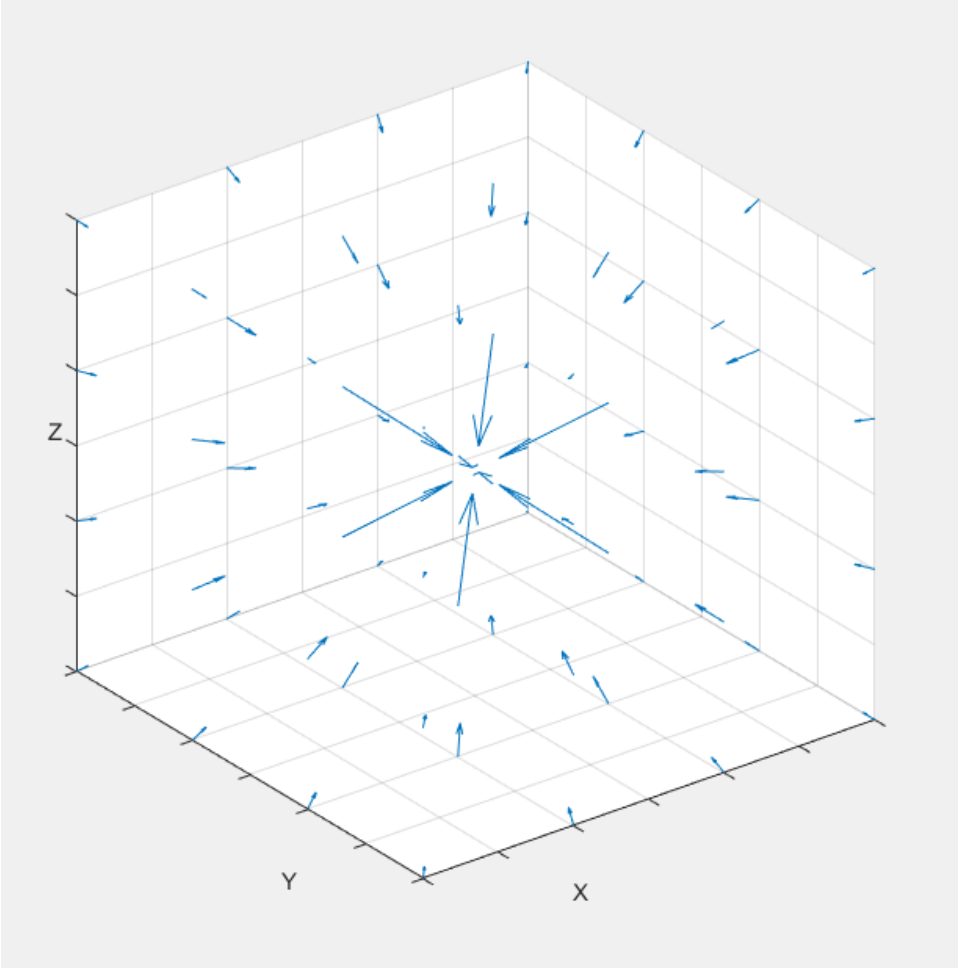

Figure 2.1: Vectors showing the vector field $\vec{g}(P)$ around a point particle

The gradient connects the vector field and the scalar field. $\nabla V(P)$ is the gradient to the scalar field $V(P)$, the vector ∇V will always stand orthogonal to the equipotential surface V [Gjevestad, 2016][Helland, 2014].

$$\nabla V(P) = \left(\frac{\delta V}{\delta x}\right)\vec{i} + \left(\frac{\delta V}{\delta y}\right)\vec{j} + \left(\frac{\delta V}{\delta z}\right)\vec{k} \tag{2.4}$$

The gravitational field is a conservative vector field, thus it can be represented by a scalar potential field. The potential $V(P)$ equals

$$V(P) = \frac{Gm}{r} \tag{2.5}$$

and it holds

$$\vec{g}(P) = \nabla V(P) \tag{2.6}$$

2.3 Superposition principle

The superposition principle is the idea that the gravitational attraction from an object is the sum of all point mass particles of the same. The total gravitational attraction of the Earth on a point P can this be written as the sum over all point masses m_i according to

$$\vec{g}(P) = -\sum_{Earth} \frac{Gm_i}{r^3}\vec{r} \tag{2.7}$$

For the representation of the gravitational field in terms of the gravitational potential V, it holds

$$V(P) = \sum_{Earth} \frac{Gm_i}{r} \tag{2.8}$$

An infinitely small mass element dm can be represented by the product of density times volume according to

$$dm = \rho dv \tag{2.9}$$

Thus (2.8) can be written in the continuous case as the integral

$$V(P) = G_{Earth} \frac{1}{r} \rho \, dv \tag{2.10}$$

2.4 Poisson's equation and Laplace's equation

Application of the Laplace operator $\Delta = \nabla^2$ (2.11) yields Poisson's equation.

$$\Delta V = \frac{\delta^2 V}{\delta x^2} + \frac{\delta^2 V}{\delta y^2} + \frac{\delta^2 V}{\delta z^2} = -4\pi G\rho \tag{2.11}$$

The density inside the earth is not constant. If we can solve Poisson's equation, we can also find the earth's gravitational field. If we know the density ρ everywhere inside the earth, we can use the super positioning principle in

(2.10) to compute the potential V. Differential equations are also better to use when facing boundary value problems. Equation (2.11) is a second order differential equation, which can be solved theoretically. In order to determine the specific solution for the Earth's gravitational field, it is necessary to introduce boundary values.

$$_S\vec{g}\vec{n}_S dS = -4\pi G_v \rho dv \tag{2.12}$$

Instead of using Poisson's integral, we can use Gauss integral. Gauss' integral connects the gravitation $\vec{g}$ and the surface S around the masses where $\vec{n_s}$ is the normal to the surface S. This is the essential equation which the earth's gravitational field can be computed from.

Point masses outside the gravitational field will behave differently. The density ρ outside the masses is 0, and this alters Poisson's equation

$$\nabla^2 V = \frac{\delta^2 V}{\delta x^2} + \frac{\delta^2 V}{\delta y^2} + \frac{\delta^2 V}{\delta z^2} = 0 \tag{2.13}$$

This form of Poission's equation is called Laplace's equation [Skaar K., 2015]. If Laplace's equation holds, the function V is a harmonic function.

2.5 Spherical harmonic function

To solve these boundary value problems for spheres, we can use spherical harmonic functions. Laplace equations rewritten as spherical coordinates, r radius, θ latitude, λ longitude, yields

$$r^2\frac{\partial^2 V}{\partial r^2} + 2r\frac{\partial V}{\partial r} + cot\theta\frac{\partial^2 V}{\partial \theta^2} + \frac{1}{\sin^2\theta}\frac{\partial^2 V}{\partial \lambda^2} = 0 \tag{2.14}$$

The solutions to this second order differential equation will normally look like this:

$$V(r,\theta,\lambda) = f(\lambda)P_{nm}(\cos\theta)g(r) \tag{2.15}$$

$$f(\lambda) = \cos\lambda,\ or\ \ f(\lambda) = \sin\lambda \tag{2.16}$$

$$g(r) = r^n,\ or\ \ g(r) = \frac{1}{r^{n+1}} \tag{2.17}$$

The function P_{nm} inside (2.15) is called Legendre polynomials and derive from series expansion of $\frac{1}{r}$

$$\frac{1}{r} = \frac{1}{\sqrt{1 + (\alpha^2 - 2\alpha u)}} \tag{2.18}$$

However equation (2.17) provides two possible solutions. One for the internal and one for the external problem. The function V will converge for one of the

two solutions. If $g(r) = r^n$, then V will converge inside the boundary (r<1). This solution belongs to the interior problem, which means that masses are only outside the sphere. The second solution $g(r) = 1/r^{n+1}$ converges for r>1, thus this case is the exterior problem, with masses insides the sphere and mass free space outside. With help from coefficients A_{nm} and B_{nm} a solution to (2.15) can be written as a series which converges outside the masses.

$$V(r,\theta,\lambda) = \sum_{n=0}^{\infty}\sum_{m=0}^{n}\frac{P_{nm}(\cos\theta)}{r^{n+1}}(A_{nm}\cos m\lambda + B_{nm}\sin m\lambda) \tag{2.19}$$

This solution is a superposition of all particular solutions, i.e. a combination of cos or sin with $1/r^{n+1}$. Basically this leads to a set of four coefficients. It then has to be decided, if the problem is an exterior or interior problem, which allows to set two sets of coefficients to zero. The remaining coefficients are A_{nm} and B_{nm}. Dirchlets problem is to figure out the potential outside the sphere S when we have the potential V on the surface. The solution is to expand the 2nd order differential equation in equation (2.19). This solution is called Poisson's integral and is an important equation in potential theory.

$$V_e(r,\theta,\lambda) = \frac{R(r^2-R^2)}{4\pi}\int_{\lambda=0}^{2\pi}\int_{\theta=0}^{\pi}\frac{V(r,\theta,\lambda)}{r^3}\sin\theta\, d\theta d\lambda \tag{2.20}$$

2.6 The earth's gravity field

Since the earth is rotating, the force on objects along the surface of the earth is not only affected by the gravitation of the earth. Additionally, the spin of

the earth influences the force of attraction towards the Earth as well. The gravity g is formed by two nature phenomena, the gravitation plus the effect from the spin of the earth.

$$g = \nabla W \tag{2.21}$$

Gravity $\vec{g}$ is what we are measuring when using gravimetric instruments. The gravity potential W is the rotational potential V_c added to the gravitation potential V.

The rotational potential depends on the rotational velocity w_e around the z axis in addition to the distance from the rotational axis.

$$V_c = \frac{1}{2}{w_e}^2(x^2 + y^2) \tag{2.22}$$

The rotational potential is a non-harmonic function since it does not fulfil Laplace's equation.

$$W = V + V_c \tag{2.23}$$

2.7 Height systems

Height systems are implemented in geodesy to find the height above an agreed upon zero height. Different height systems refer to individual surfaces, among them, the geoid is the most significant. Geodetic heights have various geometric and physical purposes. Since heights above various surfaces has to be expressed, different height systems have to be introduced.

Geopotential or the geopotential number C is used to calculate heights in different height systems. To find the geopotential number, the difference in the potential on the surface P and the potential on the geoid (O) has to be calculated. The difference is

$$C_P = W_O - W_P = -\int_O^P dW = \int_O^P g dn \tag{2.24}$$

The ellipsoid that best fits with the geoid is used when finding the normal height. The ellipsoid's gravity field is called the normal gravity field. Assuming the normal gravity field is equal to the real gravity field, the difference in geopotential (C) divided by the normal average gravity along the plumb line ($\overline{\gamma}$) is the normal height N [Yilmaz, 2008].

$$N = C/\overline{\gamma} \tag{2.25}$$

Dynamic height is calculated when dividing the geopotential C by the normal gravity value at 45 degrees latitude (γ_0) which is constant.

$$H^{Dyn} = C/\gamma_0 \tag{2.26}$$

Gravity inside the earth cannot be measured, therefore gravity has to be

computed regarding the density and mass distribution below the surface of the earth to find orthometric height. The difference along the plumb line from a point on the surface to the geoid is orthometric heights, which is "heights above sea level".

$$H^{Ort} = C/\overline{g} \tag{2.27}$$

$\overline{g}$ is the gravity computed on the geoid.

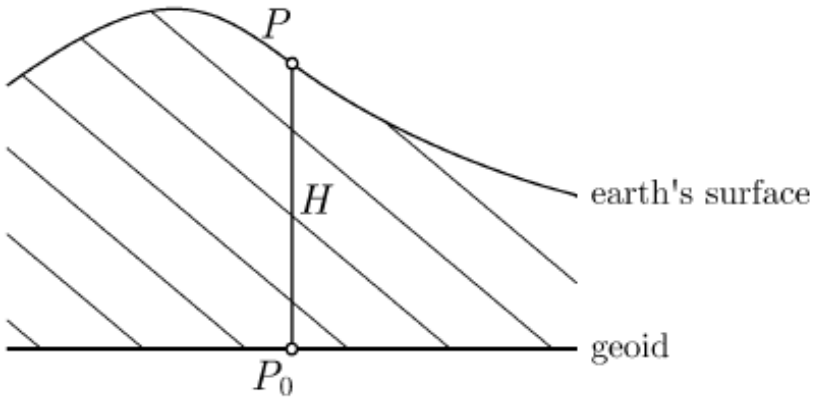

Figure 2.2: Gravity reduction down on the geoid [Yilmaz, 2008]

2.8 Calculate the geoid from GNSS and gravity observations

An important usage of the potential theory is to compute the geoid from gravity and GNSS observations.

The equations are non-linear, so they need to be linearised. In order to do so, a proper approximation is introduced. This is represented by a best-fitting ellipsoid respectively the normal field, which is the gravity field

generated by an ellipsoid of same total mass and angular velocity as the earth [Hoffmann-Wellenhoff et al., 2005]. The small rest, anomalies or disturbances are then treated by the linearised equations. Spherical approximations is applied to the equations to neglect all terms depending on the flattening of the ellipsoid.

Since we are interested in gravity field determination, we deal with equipotential surfaces. They represent the shape of the earth, because the geoid is used as boundary surface, which means there are no masses outside this boundary.

In the classical theory of Stokes, the geoid is chosen as boundary. Therefore we need to perform topographic reductions, because those masses violate the assumption that there are no masses outside the geoid.

A geoid height N is the height difference from a point (Q) on the ellipsoid to a point (P) on the geoid. Lets say W is the gravity potential and U is the normal potential

$$W_0 = W(P) = U(Q) = U_0 \tag{2.28}$$

As seen in (2.28), the gravity potential and the normal potential will be equal. g is the gravity and $\vec{\gamma}$ is the normal gravity. The connection between gravity and gravity potential and the normal gravity and the normal potential is

$$g = \nabla W \tag{2.29}$$

$$\vec{\gamma} = \nabla U \tag{2.30}$$

Disturbing potential $T(P)$ is the difference between gravity potential and normal potential:

$$T(P) = W(P) - U(P) \tag{2.31}$$

Gravity disturbance is similar to the disturbing potential

$$\delta g = -\frac{\partial T}{\partial r} = g(P) - \gamma(P) \tag{2.32}$$

while the gravity anomaly is the difference between the gravity on the geoid and the normal gravity on the surface of the ellipsoid,

$$\Delta g = g(P) - \gamma(Q) \tag{2.33}$$

The disturbing potential can also be expressed from series expansion of the normal potential U and the normal gravity γ.

$$T = \gamma N \tag{2.34}$$

Inferred from this we get Bruns formula:

$$N = \frac{T}{\gamma} \tag{2.35}$$

Bruns formula is used to compute the geoid height. Neumann-Koch's equation and Stokes' equation is used in classical geodesy to find the disturbing potential. The disturbing potential can then be divided by the normal gravity to to compute the geoid height.

This first equation is the Neumann-Koch's equation inside the integrals with respect to the gravity disturbance δg

$$T = \frac{R}{4\pi\,\sigma}\,(\frac{1}{\sin\psi/2} - ln(1 + \frac{1}{\sin\psi/2}))\delta g d\sigma \tag{2.36}$$

Stokes formula is the second way of calculating the disturbing potential. The difference is that this formula is with respect to the gravity anomaly Δg. Stokes' function is as follows:

$$S(\psi) = \frac{1}{\sin\psi/2} - ln(1+6\sin(\psi/2)+1-5\cos(\psi)-3\cos(\psi)ln(\sin(\psi/2)+\sin^2(\psi/2)) \tag{2.37}$$

Stokes' formula depends on Stokes' function

$$T = \frac{R}{4\pi} \int_{\sigma} S(\psi) \Delta g d\sigma \tag{2.38}$$

Currently, in geodesy Stokes' formula is most common to use, since most observations are acquired from GNSS measuring instruments. Hence Stokes' formula is rather important, as it can be used to calculate the geoid from gravity data.

Chapter 3

Geophysical signals, geophysical fluid dynamics, atmosphere ice and hydrology

3.1 Geophysical fluid dynamics

Geophysical fluids are described by the conservation of energy and conservation of momentum(Newtons's second law). The flow of the fluid is incompressible, which means the density ρ of the fluid varies so little that we estimate the fluid to have constant density. Extensive movements in the atmosphere like the jet stream and the gulf stream in the ocean is also a part of the geophysical fluid dynamics. These effects are caused by large constantly moving systems on earth, like temparature differences on the earth surface and the spin of the earth [Cushman-Roisin et al., 2009]. The Coriolis force is an important factor of geophysical fluid dynamics. The winds moving towards the north and the south bends towards east and west respectively. This is caused by the Coriolis effect.

3.2 Geophysical signals

Geophysical signals are the data we observe and gain from the earth. The varying signals detected from the earth is observed, processed and analysed. Signals can be passive and active. Passive signals are detected from the natural occurring signals or fields transmitted from the earth [Forte, 2016]. Active geophysical signals are human made signals which are sent out and reflected from the surface or the subsurface. Laser light, echo sounding and seismic methods are examples of active methods. Examples of passive measurement are observations of electric and magnetic fields. The gravity field is measured with passive methods, measuring the natural gravity field of the earth with satellites, relative gravimeters and absolute gravimeters. Passive methods are much cheaper and easier to use than active methods, since there are only a receiving end of the signal. These methods are also more cost and time efficient. The noise can usually not be controlled, since the source of the signal is less manageable.

3.3 Surface gravity loading effect

The effect of hydrological contribution to surface gravity fluctuations can be divided into two parts; the gravity loading effect and the gravity attraction effect. The loading effect is how the surface water storage changes the effect of gravity, which is shifting depending on seasonal differences [Yi et al., 2015]. Water storage changes deform the topography. The effect that the surface is pressed down by the weight of the hydrological masses. Therefore the gravity station is depressed as well. Gravity increases as the sensor comes closer to the Earth's center of mass. The gravity attraction effect is explained in the previous chapter.

3.4 Ocean loading and ocean tides loading

Earth and ocean tides are the rise and fall of the earth crust and the ocean because of gravitational effects. Additionally, there is an ocean loading tide effect, which is moving water masses pressing down the crust caused by the ocean tide [Timmen L., 2010]. The ocean tide load (OTL) is also caused by the redistribution of masses due to crustal deformations and the displacement of the observation point as a result of the load of the ocean [Breili, 2009]. The ocean load tide is a much smaller effect than the ocean tides, but it is still significant enough to notice when measuring with gravity instruments. The ocean load tide is not in phase with ocean tide or earth tide. All these effects will maximum amount to an effect of 300 μGal peak-to-peak. The OTL M2 (lunar) effect vary around the Earth, the amplitude effect (NAO99b model) on the surface of the Norway taken from the NAO99b model is shown in this figure:

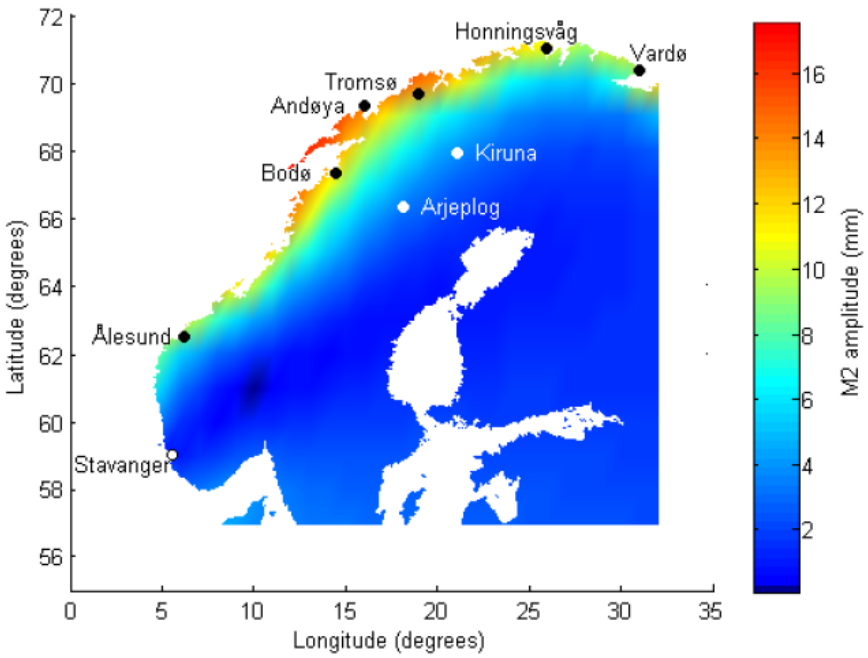

Figure 3.1: The NAO99b model predicted amplitude of the vertical deformation due to the M2 OTL constituent in Fennoscandia

3.5 Hydrological cycle

The hydrological cycle contains four parts, which are listed in order of magnitude; oceans, ice, ground water and atmosphere [Winter et al., 1998]. The evaporation from oceans and land, melting of snow and ice, rivers and groundwater which flow towards oceans, and the precipitation from the air to the land and ocean completes the hydrological cycle.

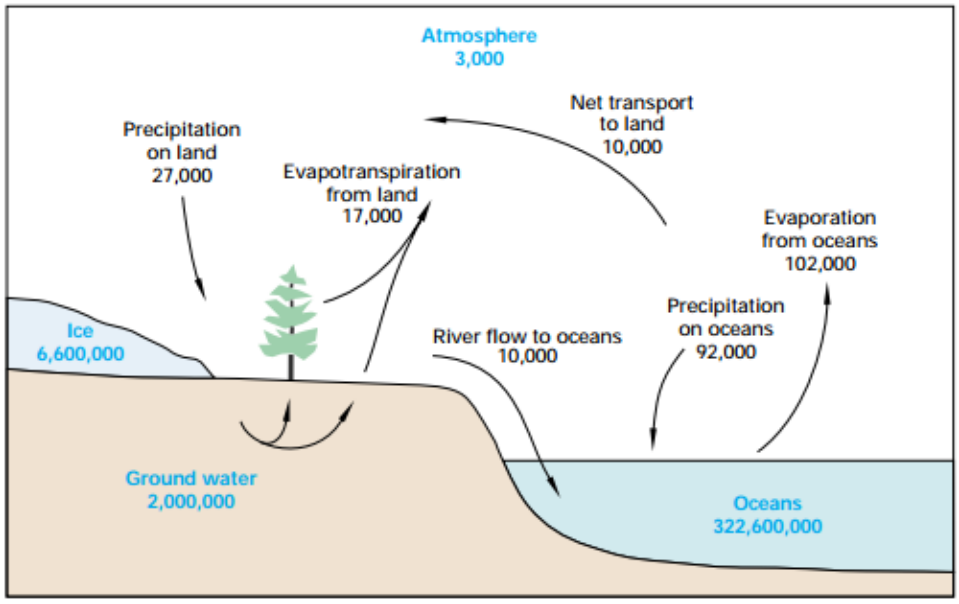

Figure 3.2: The hydrological cycle. Oceans, atmosphere, ice and ground water given in cubic miles($4.168 * 10^{12} liter$) and fluxes given in cubic miles per year. [Winter et al., 1998]

3.5.1 Groundwater

Water in the ground is quantified in different layers. When the creaks and cracks in the bedrock beneath the soil and the soil are filled up, that water is called groundwater. The groundwater table is the surface of the zone of saturation. Ground water stocks are often filled by only rainfall and snow melting in Norway [NVE, 2015]. The depletion of the groundwater goes into rivers, lakes and oceans. In periods without snow melting or rainfall, groundwater is the only source of water for many rivers. During the winter season, there is a decline in groundwater in non-coastal areas in Norway, while in coastal areas the groundwater is at its highest.

Chapter 4

Instrumentation

The gravity field observations and data is collected from height data and gravimeters of the FG5, the Superconducting absolute gravimeter and the Lacoste & Romberg relative gravimeters.

4.1 The FG5 instrument

Next, let us have a look at the FG5 instrument

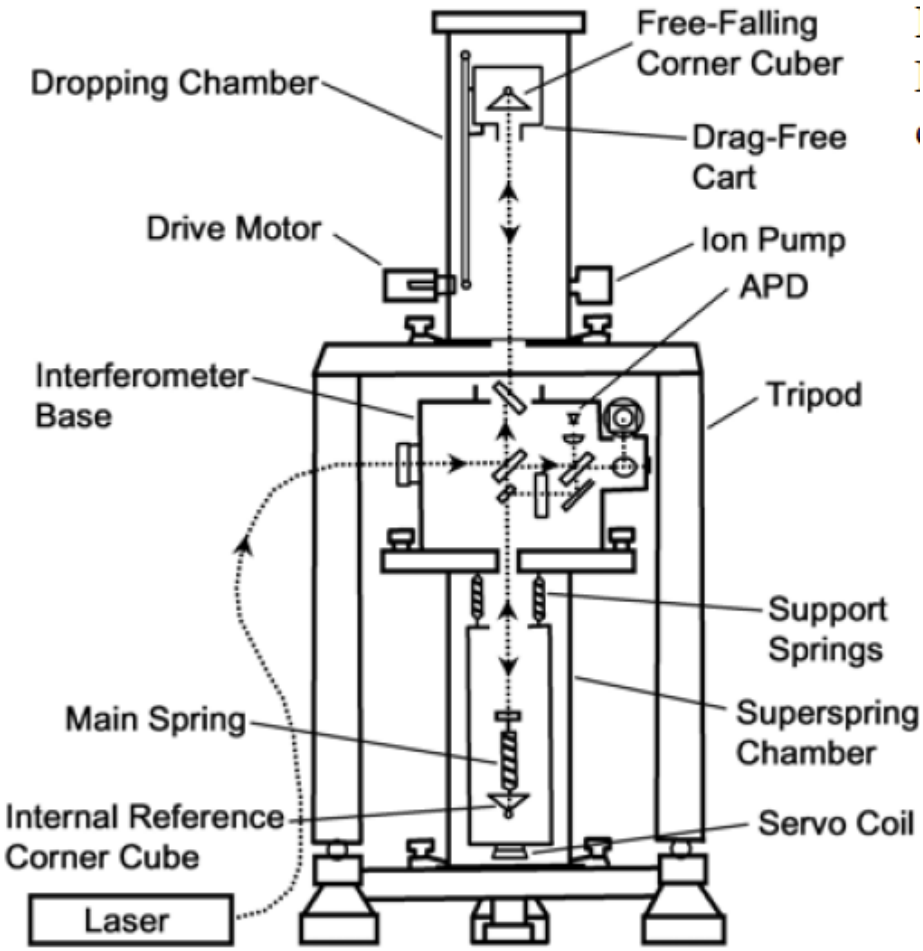

Figure 4.1: The complete FG5 instrument [Timmen L., 2010]

The FG5 instrument is an absolute gravimeter which can precisely measure gravity acceleration on the surface of the earth. It is based on the free-fall principle which employs distance and time measurements to compute gravity [Timmen L., 2010]. Inside the drop chamber in the upper half of the instrument there is a test mass which is freely falling in a vacuum. The test mass is released and will drop for approximately 200 ms. During the 200 ms a laser interferometer will execute around 600 measurements to generate ob-

servation pairs of time and distance; from those 600 pairs the gravity for that drop is estimated. One set consists 50 drops, and inside one campaign there will preferably be 24 sets (24 hours). In the lower level of the instrument there is a super spring placed. Inside the super spring there is a long period isolation spring [van Westrum D., 2001]. The isolation spring provides the inertial reference frame. It will also filter out high frequency vibrations of the instrument caused by microseismics. Without the super spring it would have been impossible to get the measurements down to $1-2\mu Gal$ accuracy.

4.1.1 Ion pump

On the side of the drop chamber there is an ion pump, which maintains vacuum inside the drop chamber. High voltage is used to ionize molecules and drift them towards a ground plate. The electron will go towards the positive plate above. Liberated electrons will also ionize other molecules which creates a pumping effect.

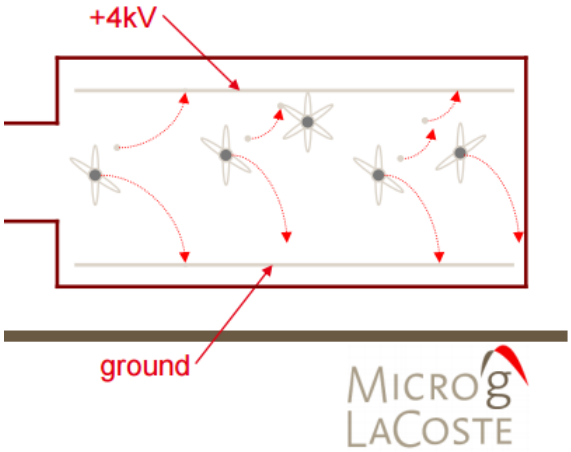

Figure 4.2: The Ion pump which pumps the ions out with high voltage [van Westrum D., 2001]

4.1.2 Interferometer

Inside the drop chamber there is a mirror in free fall, which reflects a laser beam originating from a laser. Interference fringes will be created and the interference detector will receive the signals. The interference pattern can be destructive or constructive and everything between, consequently it is possible to detect differences down to half the laser's wavelength. A photo diode will register the light intensity and transfer the information to the software, which will calculate the free fall of the upper mirror.

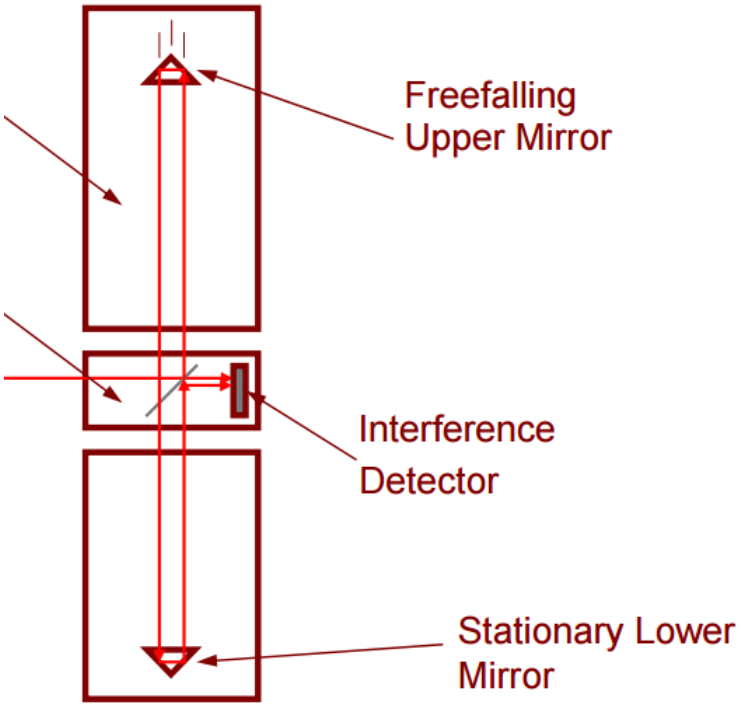

Figure 4.3: The laser goes through the falling mirror and interfere with the incoming laser into the interference detector [van Westrum D., 2001]

4.2 Relative gravimeters

A relative gravimeter does not determine gravity, it measures the difference in gravity over a time series or between two observation stations [LaCoste, 2004]. The gravity increases in average 300 $\mu Gal/m$ towards the center of the Earth. The LaCoste & Romberg instrument is created from metal parts, which means that the thermal expansion could be high. Therefore the instrument tries to maintain a steady temperature inside. The relative gravimeter is a spring-based instrument which measures the length of the spring. The length is dependent on the weight pulling the spring. The LaCoste instrument use a zero-spring because it is very sensitive to small changes in gravity. A zero-spring is a coil spring which would have had zero length if there is applied zero force.

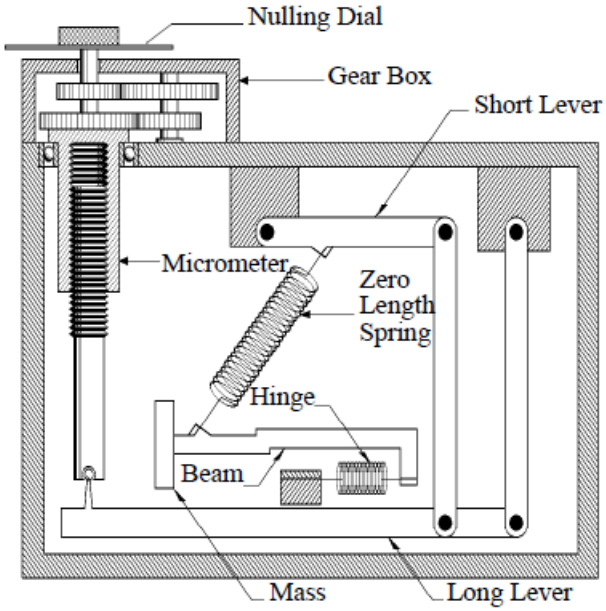

Figure 4.4: A simplified design of LaCoste & Romberg relative gravimeter [LaCoste, 2004]

The mass at the end of the beam in the relative gravimeter pulls at the

zero-length spring. At the other end of the beam is a frictionless hinge which also keeps the gravimeter from getting damaged from bumps. A high precision screw moves the levers so that the instrument can be put into reading position.

4.3 Superconducting gravimeter

The superconducting gravimeter (SG) is the most precise gravimeter which exists. The gravimeter was used when Mikolaj was developing the mGlobe program [Mikolaj, 2015]. The SG can not be moved like the FG5 instrument because it needs stability. Superconductivity has no electrical resistance, a flow of electric current on the surface of the superconductor keeps a magnet floating [Goodkind, 1999]. The magnetic field of the prior magnet is eliminated by the electric current. A magnetic levitation of a superconducting sphere is induced and the current on the surface prevents the magnet from falling down. The instrument is used for many different geophysical purposes, like tectonic movements and post-glacial rebound. The precision of the superconducting gravimeter is 0.1 μGal.

Chapter 5

Hydrological models and data

Hydrological models are simpler versions of real world hydrological cycles, though still complex for humans. Global and local hydrological models are developed to understand and anticipate hydrological processes. The most significant inputs are area of drainage and rainfall observations, other inputs are soil properties, vegetation cover, watershed topography, soil moisture content and ground water aquifer [Gayathri et al., 2015]. Soil moisture and snow depth, both in water equivalent [mm] is being analysed [Mikolaj, 2016]. The modelled soil moisture is calculated from temperature fluctuations, precipitations and observed snow depth [Mikolaj, 2015]. Mass transport in the hydrological cycle can be sensed by gravimeters. Models or observations of mass variations can be used to compute corrections of gravity time series.

Most Land Surface Models (LSMs) which are being used in this thesis was put into use January 1, 1979. These models, with one exception have 1 degree resolution. A deterministic hydrological model with same input will give same output every time, while stochastic hydrological models have some elements which is randomly determined. The hydrological gravity effect can be divided into two different categories, the gravitational attraction and the loading effect which is indirect.

5.1 Local and global hydrological contribution

Surface gravity variations are dependent on the local and the global contents of water on the surface. The hydrological contribution can be divided into the gravitational effect and the loading effect. Furthermore, the gravitational effect ($g^N(\psi)$) is the vertical attraction of the water masses, while the loading effect ($g^L(\psi)$)is the effect of the movement of the water masses (per unit mass, spherical degrees ψ from the point) [Mikolaj2, 2016].

$$g^L(\psi) = -\frac{g}{M}\sum_{n=0}^{\infty}(2h_n - (n+1)k_n)P_n(\cos\psi) \tag{5.1}$$

The load Love numbers is represented by h_n and k_n. The Earth's mass is represented by M and its mean surface gravity by g.

The "load Love number" table in the Appendix contains the load Love numbers taken from Farrell [Farrell, 1972].

The gravitational effect when the spherical distance is farther away than 1 degree is

$$g^N(\psi) = \frac{g}{4M\sin(\psi/2)} \tag{5.2}$$

Including the topography with $\psi < 1°$,

$$g^N = G\frac{(d^2 + (R+h_s)^2 - (R+h_p)^2)}{2d^3(R+h_s)} \tag{5.3}$$

The global hydrological models contains different hydrological outputs which I have chosen to use in the mGlobe software.

The GHMs used in the thesis are explained in this chapter and outputs from

Model	Outputs	
GLDAS models	Average layer soil mosture	Snow water equivalent
MERRA	Total water store in land reservoirs	
ERA Interim	Volumetric soil water layer 1-4	Snow depth
NCEP Reanalysis2	Soil moisture layers, 1-10cm, 10-200cm	Water equiv. of snow depth
GRACE-Land	Total water storage in cm	
NVE's HBV model	Variations in groundwater storage	

Table 5.1: The outputs from the various GHM

them listed in table 5.1

5.2 Model from NVE

The groundwater model from NVE (Norwegian Water Resources and Energy Directorate) is a customization of the HBV (Hydrologiska Byråns Vattenbalansavdelning) which the Swedish Institute of Meteorology and Hydrology developed [HBV model, 2015]. The HBV model is recognised as satisfactory model when comparing to other hydrological models as it is used internationally. A simplified mathematical model is produced from the hydrological natural system. The HBV model is a rainfall and run-off model which uses measured air temperature and rainfall to calculate drainage. Snowfall is a rather important factor when considering drainage within an area. The water from the rainfall or snowfall is stored as snow or as soil water, thereafter the water can go through groundwater, streams, rivers, and lakes before going out of the drainage area.

The NVE hydrological effect in this master thesis uses the groundwater content measured as water equivalent in mm, as if the groundwater was measured without the filled up soil and bedrock between it. With 1 km resolution and a 50x50 meter height model(described later), the gravity calculations closer to the gravity stations will be much more detailed than with the GHMs. The time resolution is 1 day and outer threshold is tested for 0.05 and 0.1 spherical degree.

5.3 The Global Land Data Assimilation System GLDAS

The National Aeronautics and Space Administration (NASA), Goddard Space Flight Center (GSFC), the National Oceanic and Atmosphere Administration (NOAA) and National Centers for Environmental Prediction (NCEP) have developed GLDAS together. Ground-based observations and satellite data together with advanced surface modelling and data assimilation techniques are being used to create GLDAS GHMs [Rodell et al, 2004]. The GLDAS models consist of states and fluxes of the Earth's surface around the globe. Different water resources applications, water cycle analysis and climate and weather predictions are supported by the GLDAS products. These elements and that they are being high resolution, global and uncoupled to the atmosphere is what makes GLDAS special. The GLDAS models consist of Noah, Mosaic, the Variable Infiltration Capacity model (VIC) and the Community Land Model (CLM) [Fang et al., 2009]. Every GLDAS model uses 1 degree resolution except the NOAH(0.25°), which uses 0.25 degree resolution. The depth of each layer and the number of layers are different for each model. The time resolution for GLDAS is 3 hours. In *mGlobe* 1 day resolution is chosen for all the GLDAS models. The water stored in the vegetation is neglected for all the GLDAS models, since it has an impact of less than 0.01 *muGal*.

CLM 2.0 (10 layers)	
Depths	0-0.018, 0.018-0.045, 0.045-0.091, 0.091-0.166, 0.166-0.289, 0.289-0.493, 0.493-0.829, 0.829-1.383, 1.383-2.296, and 2.296-3.433 m.
MOS (3 layers)	
Depths	0-0.02,0.02-1.50, and 1.5-3.50 m.
NOAH (4 layers)	
Depths	0-0.1, 0.1-0.4, 0.4-1.0, and 1.0-2.0 m.
VIC (3 layers)	
Depths	0-0.1, 0.1-1.6, and 1.6-1.9 m.

Figure 5.1: The soil layer depth of the different GLDAS LSMs [Fang et al., 2009]

The Noah model is developed by a cooperation between researchers from

private and governmental institutions; the Global and Continental-Scale International Project (GCIP) and NCEP to establish a modern LSM for usage in climate and weather prediction models in NCEP. The Noah is still being improved. The CLM model is made by a community of scientists who are not being controlled by a government or organisation. The model is made of the best components from NCAR's LSM, the Biosphere-Atmosphere Transfer Scheme (BATS) and the LSM of the Institute of Atmospheric Physics of the Chinese Academy of Sciences. Mosaic model is established with the purpose of making mosaic tiles with vegetation classes within the grid cells. The VIC model is being used in agricultural project as it functions well in moist places.

5.4 The MERRA-Land

The Modern-Era Retrospective Analysis for Research and Applications(MERRA) is a leading edge reanalysis that produce hydrological cycle data from 1979 through present date [Reichle et al., 2011]. The state-of-the-art GEOS-5 data assimilates a climate framework through including different modern observing system. The MERRA-Land data product contributes a set of hydrological land surface fields, and additionally uses Incremental Analysis Updates (IAU) to gradually fit the model towards the observations. MERRA-Land precipitation forcing is based on combining MERRA precipitation with a gauge based data product from MERRA NOAA Climate Prediction Center. Within surface hydrological modelling, precipitation is clearly the most influential parameter, therefore the MERRA-Land is constructed. The MERRA-Land data mostly turn out to be more precise than the original MERRA data.

5.5 ERA Interim

ERA Interim-Land is a global reanalysis of land surface parameters using forcing from ERA Interim, which is a global atmospheric reanalysis tool [Dee et al., 2011]. ERA Interim is produced by the European Centre for Medium-Range Weather Forecast (ECMWF). ERA Interim-Land is modified for precipitation adjustments. The time resolution of ERA Interim is 6 hours and the spatial resolution is 80 km. The analysis take measurement data and incorporate it with previous forecast model data. Thereafter the analysis estimates the variance in the global atmosphere and the global LSM. In the end it creates a forecast model for the next 12 hour cycle.

5.6 NCEP Reanalysis-2

The National Centers for Environmental Prediction NCEP Reanalysis-2 is an upgraded version of the NCEP Reanalysis-1. The updated version has fixed data assimilation errors, more data included and better physical parametrization is included [NCEP Reanalysis, 2017]. The NCEP Reanalysis has a broad observational database for use in climate monitoring and other research. Some inputs in the reanalysis are data from aircraft, satellites, ships, rawinsondes and wind speed observations [Kalnay et al., 1996]. The outputs snow depth and soil wetness from the NCEP reanalysis are not directly affected by observational inputs and are derived from the model. NCEP has a time resolutions of 4-times a day, daily and monthly values from 1979/01 to 2016/12. The soil moisture output from 0-10 and 10-200 cm and snow depth water equivalent is only given as 4-times daily values or monthly.

5.7 GRACE-Land

The Gravity Recovery and Climate Experiment (GRACE) is observing Earth's changes in the gravitation potential. The terrestrial water storage (TWS) is calculated after taking account for and removing the oceanic and atmospheric effect [Landerer et al., 2012]. To create a total water storage model, spherical harmonic coefficents are derived from model data. Following, the coefficients are rescaled to the 1x1 latitude/longitude to evaluate the fading of the signal due to noise and observation errors. The spatial resolution for GRACE data is not as high as other hydrological models, therefore the differences between the data sets have to be resolved before analysis can be done.

5.8 Atmospheric models

European Centre for Medium-Range Weather Forecasts (ECMWF) is an international organization which runs the biggest weather prediction data center in the world[http://www.ecmwf.int/en/about/who-we-are]. From ECMWF ERA Interim analysis data is used to calculate the local and global atmospheric effect. The atmosphere is modelled by pressure levels, whereas density variations are calculated from temperature, specific humidity and pressure given by the ECMWF ERA Interim models. These models have 37 levels from 1000 hPa to 0.1 hPa. The grid size for the ERA Interim data is 0.75x0.75 degrees, type of level equals pressure level. The time of hour must equal 0,6,12 or 18 since the data has 6 hour sampling. To calculate atmospheric gravity variations the data of geopotential, specific humidity, temperature, surface data and orography has to be downloaded from ECMWF. The height is calculated after dividing by 9.80665 nm/s^2.

Chapter 6

Matlab and mGlobe

Matlab is used to download and compute the local hydrological effect from the groundwater given by NVE. The *mGlobe* program is a software created in Matlab with many different functions and tools which are being used to estimate the gravity effects and variations from atmospheric models, global hydrological models and ocean models. Since many of the models have different format and resolution, *mGlobe* can be used to transform the different formats into mat-format which Matlab uses. Hence, the different models can be used in the same type of computations, and be compared to each other.

mGlobe uses models from several organisations. The data is mainly being downloaded through different national and international websites as described in the previous chapter. To calculate the gravity effect, different types of raw data has to be taken into consideration. There are three types of models in *mGlobe* that are used; hydrological models, ocean models and atmospheric models. Hydrological models are used in this thesis to calculate the hydrological gravity attraction.

6.1 Download groundwater data from NVE

The function *nvedownload* reads variations in groundwater storage from NVEs hydrological run-off model and stores them in a Matlab struct called *dat*.

The function *nvedownload* is not a part of the mGlobe program. It is a self made program which outputs total water storage variation in mm for every day from 2014 to 2017. The inputs for the function is start and end of the period (both year, month and day) and UTM zone 33N coordinates X and Y [m] for the selected site (p). 'http://h-web02.nve.no:8080/Api/GridTimeSeries/' is the url which the data is being downloaded from (Appendix). The output is the struct *dat* with *month*, *day*, *ut* (universal time), *JD* (Julian day number) and *gwbgwt* (total groundwater storage variation [mm]).

To download the data with the *nvedownload* function for different grid cells (i), I made a loop which moves the position of the download site. A double for-loop where i goes through the X-coordinates and j goes through the Y-coordinates. Inside the loop, *nvedownload* runs with a new position every time, however with the same time period as last time going through the loop. If a number in *dat.gwbgwt* is higher than 10,000, the loop changes that number to NaN (not a number). Originally, the *nvedownload* function crashes if there is ocean or no data in the cell it is trying to download groundwater variation from. Therefore the loop consists of a "try and catch" process, which ignores the error, set that cell to NaN and continue the loop. Consequently that cell is not considered in the computation. Thereafter the groundwater variations for that square kilometer is saved into the 3-dimensional matrix. The 3 dimensional matrix consists of a grid cell map in the xy-plane, and number of days along the z-axis. Thus the groundwater storage is stored in a map with a new layer for each day.

After the 3-dimensional map is transferred in the script, a movie which updates the map every day is created as showed in the figure below, with 7x7 km for simplification.

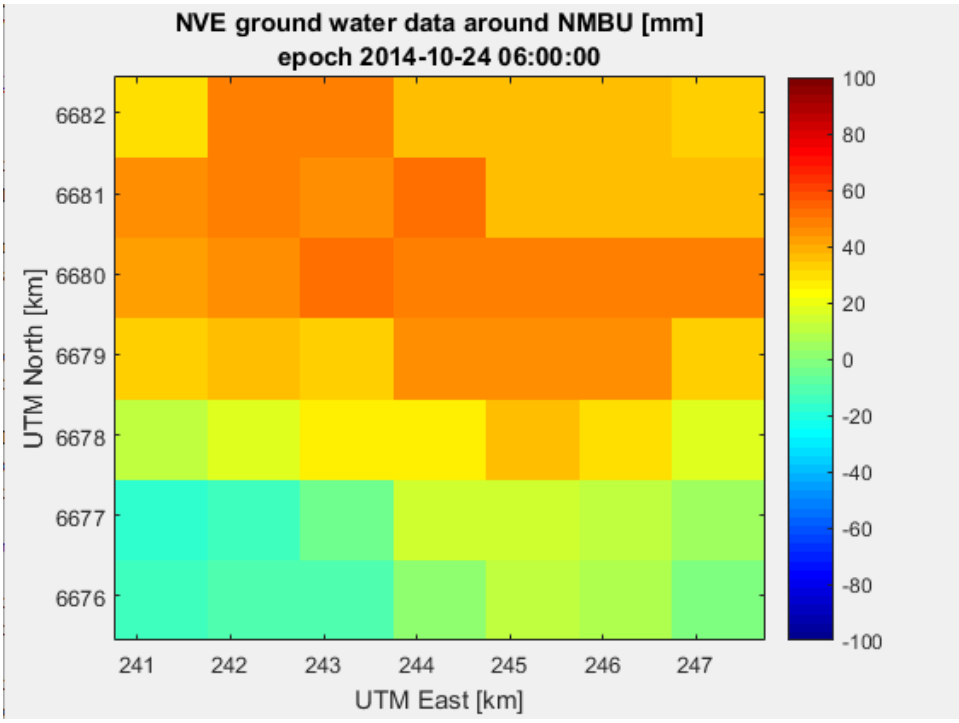

Figure 6.1: The groundwater 24th of October, 2014 within 7x7 km grid, NMBU gravity point in the center cell

6.2 mGlobe Local gravity correction

To find the gravity attraction effect as regards the groundwater storage, the downloaded data from NVE must be multiplied with the area of the corresponding grid cell. If the downloaded groundwater content for one day is 1 mm, the mass of that water multiplied with 1 square km ($10^6 m^2$) equals

$$M = 0.001m * 1000kg/m^3 * 1,000,000m^2 = 1,000,000kg$$

The weight of 1 cubic meter of water is 1000 kg. Hence, the gravitational effect of water along the connection line if it is a distance of 10 km from the point(r_{pi}) equals

$g = Gm/r^2 = 6.674215 * 10^{-13} m/s^2$

The gravitational attraction along the plumb line has to be calculated with height difference and curving of the Earth taken into account. Data on the depth of the groundwater is not available, therefore the groundwater data for each cell is stored on the surface of the DEM.

The *mGlobeLocal* script is used to calculate the loading and gravitational attraction respons to 1 mm water in each grid cell it contains. The gravity loading correction and the gravity attraction correction is given in $\frac{m}{s^2}/\frac{kg}{m^2}$. It consists of a DEM file (input) and spherical approximation to calculate the gravity impact. The inputs are positions as well as height of the point of observation, a polygon with maximum and minimum longitude and latitude, grid resolution, the table *mGlobedatadgEHydro* with spherical distance and loading effect for 1 kg of load and finally the replacement sphere radius and inner and outer threshold in spherical distance. The inner threshold is implemented to avoid that the closest cells to have too short distance to the point of observation. The outer threshold have to be less than 1 spherical degree to keep the gravitational effect local and limit the computational burden.

Showing how the local function works, a small example is showed. $Surface$ is the area with mass which is calculated inside *mGlobeLocal*. If $surface$ is small and with a long spherical distance (r_{pi}), correspondingly, the gravity response of that cell is small.

Further, to find the gravity loading correction (dgE), *psiint* is introduced. *psiint* is the interpolated gravity loading effect for the spherical distance.

$$dgE = psiint * surface \tag{6.1}$$

The heights which are obtained from the DEM are interpolated on the chosen grid size. To find the gravity attraction correction (dgP) for one grid cell,

this equation that follows is implemented:

$$dgP0 = G * surface/r_{pi}^2 \tag{6.2}$$

$dgP0$ is the attraction towards the surface, while dgP is the part of attraction which is in vertical direction. dgP is calculated on page 44.

$$\cos(\alpha) = \frac{r_{pi}^2 + (r + hD)^2 - (r + hreg)^2}{2r_{pi}(r + hD)} \tag{6.3}$$

To find the gravitational impact towards the center of the Earth for that surface, the attraction is resolved. hD is the height of the observation point and $hreg$ the height of the $surface$. The part of the vertical component of the earth is dgP.

$$dgP = -dgP0 * \cos(\alpha) \tag{6.4}$$

Figure 6.2 show the Earth(sphere), the vector from the center of the Earth to the surface and the vector from the center of the Earth to the observation station. The vector between the observation station and the center of the surface is also shown.

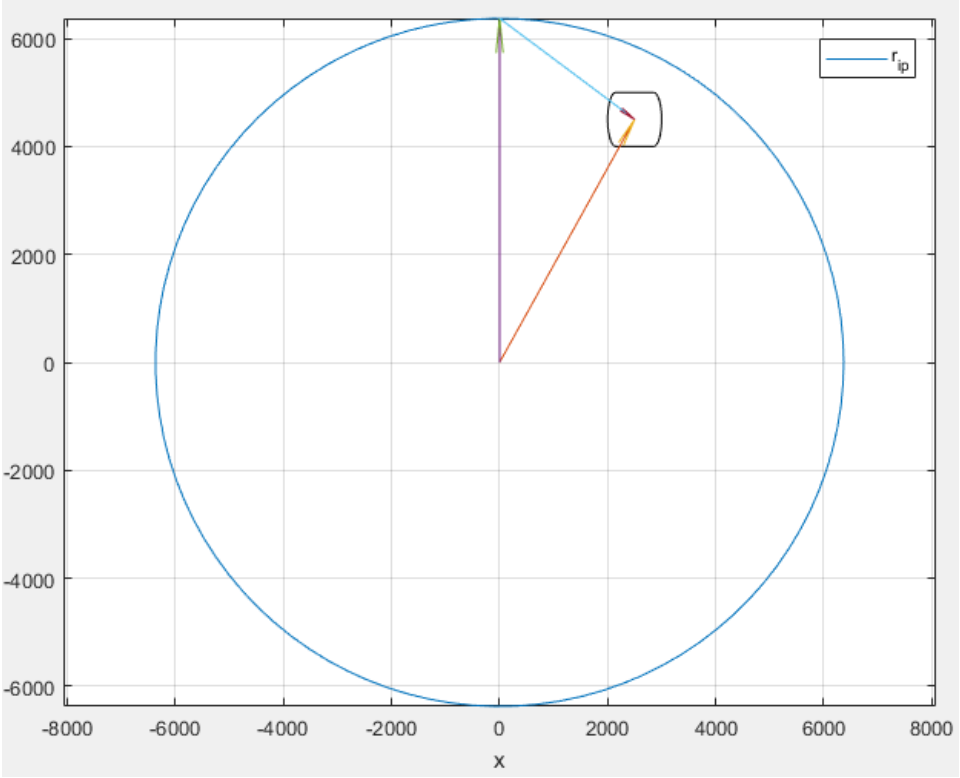

Figure 6.2: vectors between the surface tile and point of observation (r_{pi}), center of the earth and point of observation ($hD+r$) and center of the earth and center of the surface ($r+hreg$), (x- and y-axis in km)

To create a simplified example let us use a 15x9 grid with center point latitude 67.280 and longitude 14.395 degrees (cell [8,5]). The cell size is 0.0090 degrees in latitude and longitude direction, or approximately 1 km in latitude(x) and 0.39 km longitude(y). The $surface$ size for every grid cell is then roughly 39,000 square meters. Let us say the height (z) of the cell is 0 meters and the height of the observation point is 60 or 200 meters. The distance from the observation point to the center point of the corner i (position [1,1]) is

$r_{pi} = sqrt(X^2 + Y^2 + Z^2) = sqrt((4y)^2 + (7x)^2 + 60^2) = 4843m$

for $hD = 60m$, $x = 1000m$ and $y = 390m$. F

or $hD = 200m$, r_{pi} equals

$r_{pi} = sqrt(X^2 + Y^2 + Z^2) = sqrt((4y)^2 + (7x)^2 + 200^2) = 4847m$

When neglecting the curving of the earth. The gravitational attraction of that cell is then

$dgP0_{hD=60} = G * surface/r_{pi}^2 = 1.1089 * 10^{-12} \frac{m}{s^2} / \frac{kg}{m^2}$.

$dgP0_{hD=200} = G * surface/r_{pi}^2 = 1.1089 * 10^{-12} \frac{m}{s^2} / \frac{kg}{m^2}$.

and

$dgP0_{hD=60} = G * surface/r_{pi}^2 = 1.1089 * 10^{-12} \frac{m}{s^2} / \frac{kg}{m^2}$.

To find the vertical component of gravitation, $dgP0$ has to be multiplied with $cos(alpha)$, alpha is the angle between the vector from the center of the Earth to the point of observation $(hD + r)$ and the vector between point of observation and center of the surface tile (r_{pi}) as shown in figure 6.2.

For observation point $hD = 60$ and $hreg = 0$ $\cos(\alpha) = (r_{pi}^2 + (6371000 + 60)^2 - (6371000 + 0)^2)/(2 * r_{pi} * (6371000 + 60)) = 0.012800$

The gravitational attraction along the plumb line is then

$dgP_{hD=60} = -dgP0 * \cos(\alpha) = -1.4146 * 10^{-14} \frac{m}{s^2} / \frac{kg}{m^2}$

For observation point $hD = 200$ and $hreg = 0$ $\cos(\alpha) = (r_{pi}^2 + (6371000 + 200)^2 - (6371000 + 0)^2)/(2 * r_{pi} * (6371000 + 200)) = 0.041600$

Since the height difference is greater, proportionally the gravity attraction effect along the plumb line is greater too

$dgP_{hD=200} = -dgP0 * \cos(\alpha) = -4.6177 * 10^{-14} \frac{m}{s^2} / \frac{kg}{m^2}$

Furthermore, comparing to the values given by the $mGlobe_Local$ function,

the longitude 14.458, latitude 67.316, which results in approximately the same distance as the example above. The height at that position is 43 meter. Height difference between the position and observational position is $\delta H = 13 - 43 = -30m$. The gravity attraction correction for that position is $6.2322 * 10^{-}15m/s^2$, which seems ok considering the 60 m height difference for the same distance gives $dgP_{hD=60} = -1.4146 * 10^{-14} \frac{m}{s^2} / \frac{kg}{m^2}$

The examples show that change in height between the different grid cells and the observation point will correlate with the change in gravitational attraction along the plumb line.

6.3 Total gravitational effect

After the groundwater data was downloaded from NVE and the impact of 1 mm with groundwater had been calculated for each grid cell, the next step was to compute the total gravity attraction correction and total gravity loading correction. I made a script called *nvelocal* which multiplies the downloaded NVE groundwater variation content (mm) with the gravity attraction and loading effect for 1 mm. This is done for each day from the beginning of 2014 to the end of 2016.

The NVE and the mGlobe grids need to be interpolated, to ensure they are in the same coordinate frame. Afterwards values from the mGlobe grid is interpolated to the location of the NVE grid points. This means, that the mGlobe grid points is available in a regular grid. Therefore interpolation is carried out in geographic coordinates. This is done with *meshgrid* and the interpolate function *interp*2 which is built in functions in Matlab. The two grids before the interpolation is showed in the figure below.

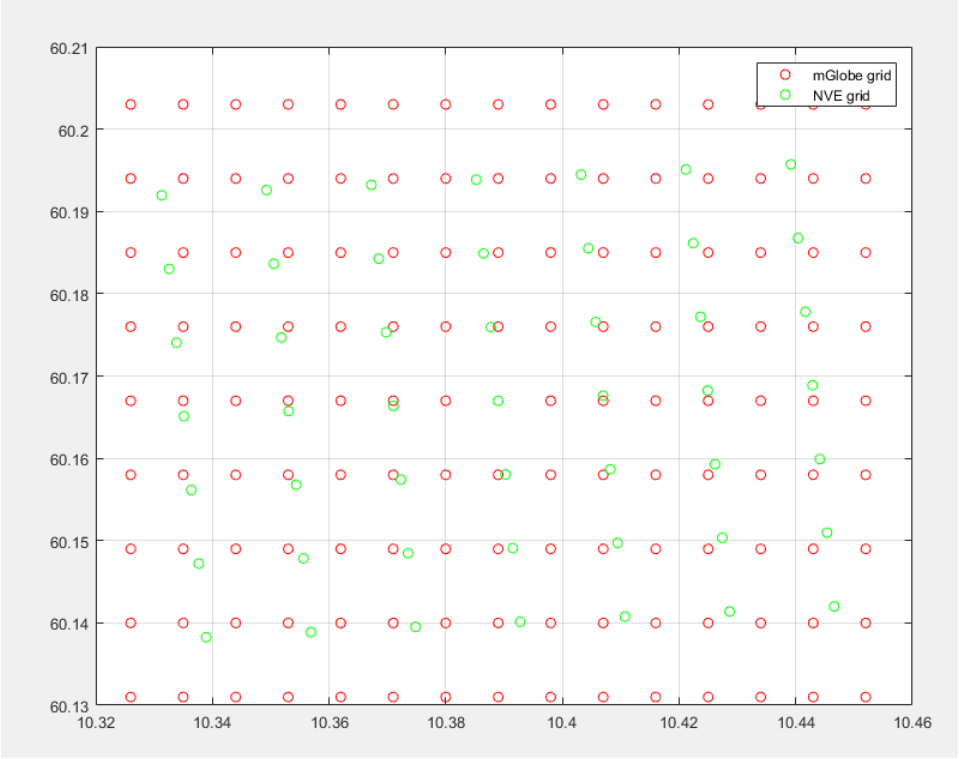

Figure 6.3: Green and red points are the center coordinates(NMBU) of the 1x1 km grid cells and 0.009 longitude(x-axis) and latitude(y-axis) degrees respectively. The groundwater content and map coordinates is interpolated later in the script to 1x1 km

To calculate the gravity attraction correction and gravity loading correction, the mGlobe Local data is multiplied element-wise with the NVE data. $dgPfinal$ is the matrix containing the gravity attraction correction and $dgEfinal$ is the gravity loading correction. They contain a time series of matrices, where each matrix represents the spatial distribution of loading and gravitational effect of the respective grid cells to the effect at the observatory in the center of the area. Therefore, the complete gravity correction at the observatory on any day is given by the sum of all grid cells every day. The final lists $dgPfinalsum$ and $dgEfinalsum$ contains the gravity attraction and gravity loading correction for every day from the start of 2014

to the end of 2016. The gravity correction $dgPfinalsum$ were 1/10th of the loading correction inside of the grid. That is because the inner cell is not accounted for when calculating the loading and attraction correction. The correction when inner threshold is 500m and inwards is the same as when the inner threshold is 0m in the *mGlobeLocal* function. That means that the groundwater closest to the station is not accounted for when calculating the gravity correction. Since the attraction correction has a large impact if the distance is small, the prism method explained in the next section is used to compute the inner most attraction correction.

The gravity variation for 3 years is analysed and compared against the global hydrological models in the signals and computations chapter.

6.4 Prism method

Since the groundwater data within 500 meter radius from the observation point in the *mGlobeLocal* function is not accounted for, a prism with the groundwater beneath the observation point is implemented, which means the DEM is not used for that area. The prism method calculates the impact the masses within a prism has on gravity. The distance and orientation from the observation point to the prism and density and volume of the prism decides the impact on gravity. To compute groundwater gravitation impact $\vec{g}$ on the gravity, a prism of mass is implemented [Tsoulis, 1999].

$$\vec{g} = G\rho_{xyz}\frac{z}{r_{Pi}^3}dx_i dy_i dz_i \tag{6.5}$$

r_{pi} is the distance between the computation point P and all the points (i) computed for.

$$r_{pi} = sqrt(x_i^2 + y_i^2 + z_i^2) \tag{6.6}$$

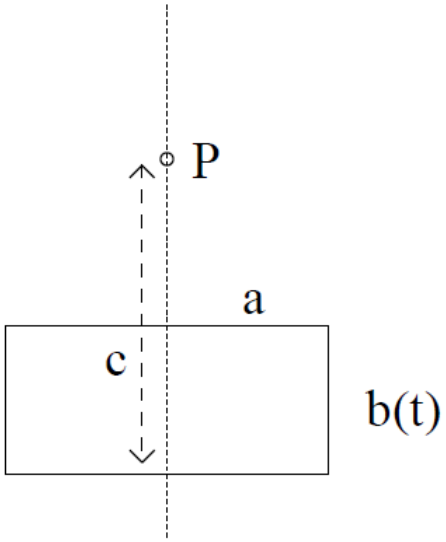

Figure 6.4: The prism fills the groundwater 1 km around the observation point. P is the observation point, a is the length from P to the border of the prism, c is the height difference between the observation point and the bottom of the prism. $b(t)$ is the groundwater equivalent in mm and it changes with time [Breili, 2009].

I chose the groundwater table or top of prism to be 10 meters below the observation point. The change from 1 to 20 meters below the ground had only an impact of 7 percent on the gravitational attraction from the prism, which means the depth of the groundwater table has less impact than how much groundwater is in the ground. The gravity loading correction for the inner zone does not have a high impact, so it is not a priority. The numerical effect may also be compared to a Bougue plate.

6.5 mGlobe Hydro

In the Hydro window in mGlobe, the inputs are the position of the observation station, the time epoch, the GHM with or without ocean layer from

mass conservation. The water in the hydrological models increases with time, therefore to minimise this continent-ocean exchange effect, the ocean layer from mass excess can be chosen. This means that a variable water layer is put over the ocean [Mikolaj, 2016]. A global DEM up to 1.05° can be chosen for implementing a rough topography. An inner threshold for the GHM also has to be chosen. The inner threshold decides the spherical degree distance from the observation point and outwards. In that area, the GHM will be counted for. Inside the threshold the LHM will be implemented.

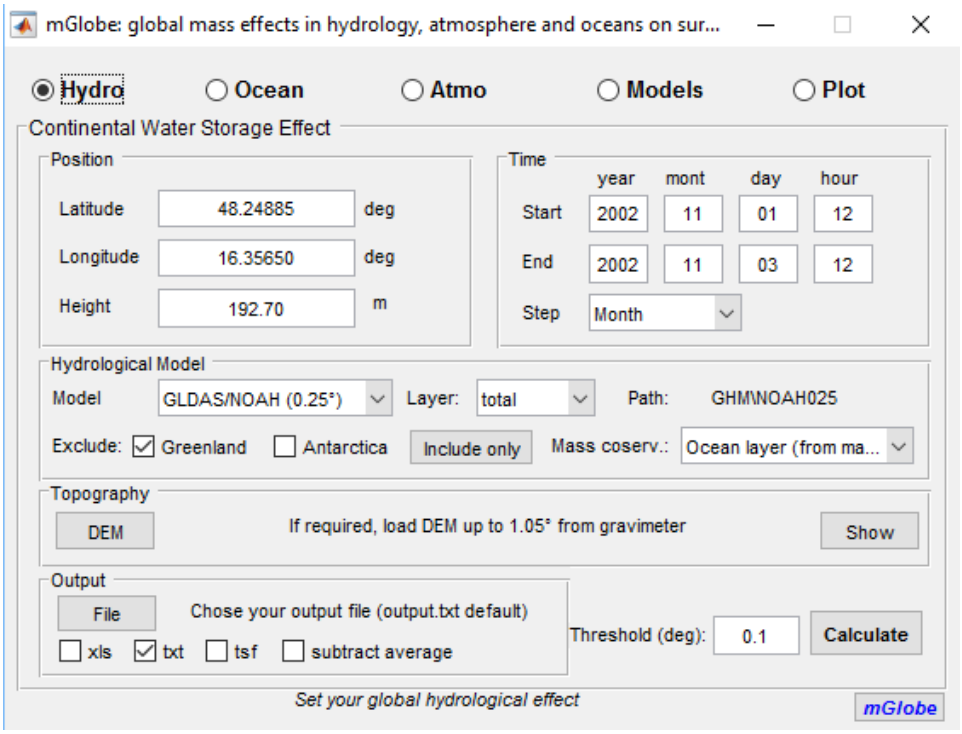

Figure 6.5: Computing the hydrological effect for observation station. The time epoch, model, mass conservation, DEM and threshold will be experimented with,

The mGlobe models can be downloaded through the websites given in the mGlobe user manual (figure 6.6) [Mikolaj, 2016].

Model	time resol.	Format	Download via
GLDAS/CLM	3 hours	-	disc.gsfc.nasa.gov/SSW/#keywords=GLDAS_CLM10SUBP_3H, or keywords=GLDAS_CLM10_M
GLDAS/MOS	3 hours	-	disc.gsfc.nasa.gov/SSW/#keywords=GLDAS_MOS10SUBP_3H, or keywords=GLDAS_MOS10_M
GLDAS/NOAH025	3 hours	-	disc.gsfc.nasa.gov/SSW/#keywords=GLDAS_NOAH025SUBP_3H, or keywords=GLDAS_NOAH025_M
GLDAS/NOAH10	3 hours	-	disc.gsfc.nasa.gov/SSW/#keywords=GLDAS_NOAH10SUBP_3H, or keywords=GLDAS_NOAH10_M
GLDAS/VIC	3 hours	-	disc.gsfc.nasa.gov/SSW/#keywords=GLDAS_VIC10_3H, or keywords=GLDAS_VIC10_M
MERRA/Land	1 hour	-	disc.gsfc.nasa.gov/SSW/#keywords=MAT1NXLND, or keywords=MATMNXLND
NCEP Reanalysis-2	6 hours	NetCDF	http://www.esrl.noaa.gov/psd/data/gridded/data.ncep.reanalysis2.gaussian.html
ERA Interim	6 hours	NetCDF	http://apps.ecmwf.int/datasets/data/interim-full-daily/
GRACE/LAND	≈month	NetCDF	ftp://podaac-ftp.jpl.nasa.gov/allData/tellus/L3/land_mass/RL05/netcdf/
Other models	3 hours	txt	-
ECCO-JPL	month	txt	ftp://podaac-ftp.jpl.nasa.gov/allData/tellus/L3/ecco_obp/
ECCO-JPL	12 hours	NetCDF	ftp://snowwhite.jpl.nasa.gov/data4/KalmanFilter
ECCO2 (beta)	24 hours	NetCDF	ftp://ecco2.jpl.nasa.gov/data1/cube/cube92/lat_lon/quart_90S_90N/PHIBOT.nc/
GRACE/OCEAN	≈month	NetCDF	ftp://podaac-ftp.jpl.nasa.gov/allData/tellus/L3/ocean_mass/RL05/netcdf/
OMCT	6 hours	txt	http://isdc.gfz-potsdam.de
		txt	ftp://podaac-ftp.jpl.nasa.gov/allData/grace/L1B/GFZ/AOD1B/RL05
Other models	3 hours	txt	-
ERA Interim (atmo)	6 hours	NetCDF	http://apps.ecmwf.int/datasets/data/interim-full-daily/?levtype=pl/
MERRA (atmo)	6 hours	nc & hdf	http://disc.sci.gsfc.nasa.gov/daac-bin/FTPSubset.pl?LOOKUPID_List=MAI6NPANA

Figure 6.6: List of supported models in mGlobe [Mikolaj, 2016]

6.6 DEM

The observation points I have chosen from the artcle which Ophaug et al.,[Ophaug et al., 2016] wrote, have different terrain characteristics around them. The NMBU station has flat terrain around it, Jondal 2 and Bodø has mountains, ocean and fjords around it, while the topography around Trysil and Ringkollen is hilly. The positions of the observation stations are as follows:

Site	$\phi(°)$	$\lambda(°)$	$H(m)$
Bodø Bankgata	67.280	14.395	13
Jondal 2	60.286	6.246	52
Trysil	61.423	12.381	693
Ringkollen	60.167	10.389	604
Ås NMBU	59.666	10.778	95

Table 6.1: Observation points

For the global DEM, the rough ETOPO1 model is used. For the local computations a more detailed DEM from Kartverket (Norwegian map authority) with 50 meter resolution is implemented.

6.6.1 Global DEM

ETOPO1 is a global relief model which combine land topography and submarine topography[Amante et al., 2009]. Only the land topography is used in this master thesis, since the ocean is put to zero values. The global relief model has a 1 arc-minute resolution. The model integrates various regional and global data sets. The "Ice Surface" version of the relief model is used, although that does not matter since only the ice surface from Greenland and Antarctic is removed in the bedrock model. ETOPO2 and ETOPO5 are the old version of the model(2 and 5 arc-minute resolution). All the ETOPO versions are created by NOAA.

ETOPO1 is the DEM used when computing the global hydrological effect. I cut out the ETOPO1 model around Norway with the web-GIS tool on NOAAs internet map page. Thereafter, I chose to download the map in xyz-format, and converted it to mat-format with $mGlobe - Models$.

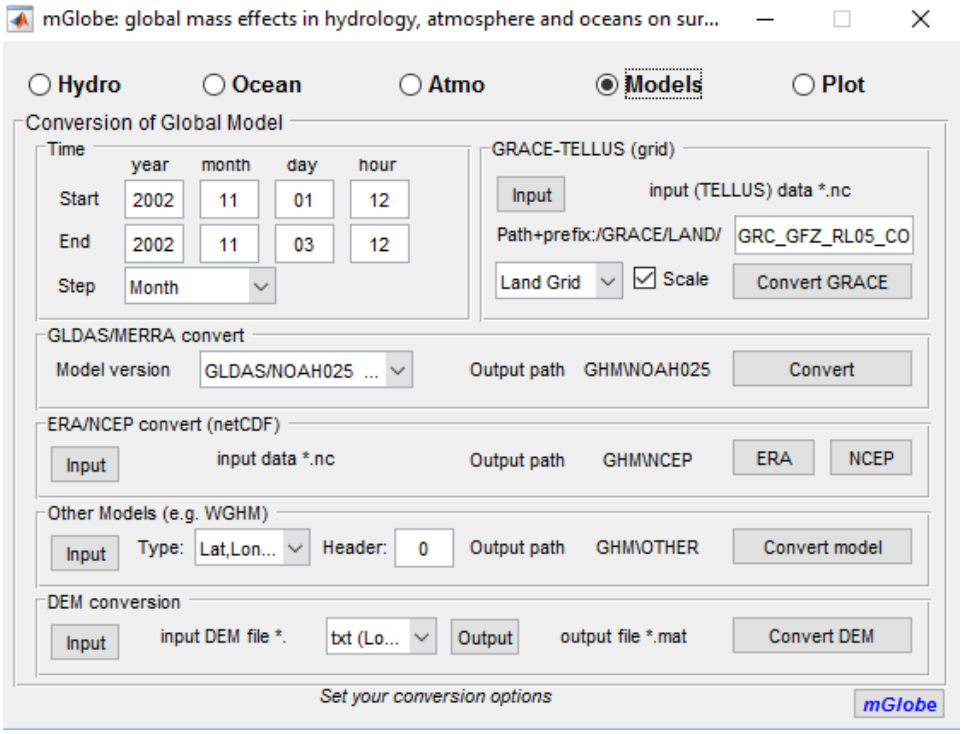

Figure 6.7: The mGlobe model window, which can convert various GHMs and DEM to mat-format

The DEM mat-format requires zero values over seas and oceans, but ETOPO1 displays the ocean topography with negative height values. Therefore I made a script *DEMheights* which changes all negative values in the DEM to zero as shown in the figure below. This script will also display an error if one or several heights are above 10,000 meters. The map is displayed below.

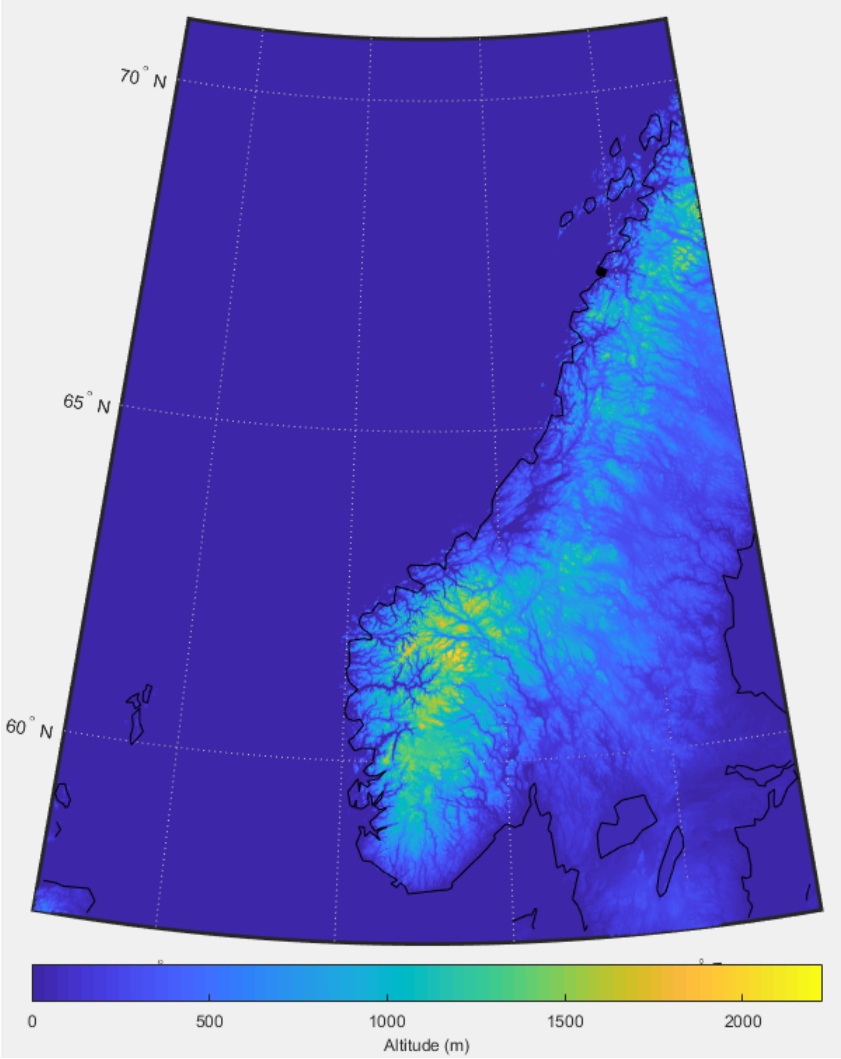

Figure 6.8: The DEM used for GHM gravity variations

6.6.2 Local DEM

The local and more detailed map is used up to 0.05 or 0.1 spherical degree from the observation point. I used QGis to convert the DEM maps from GeoTiff to ascii format, which mGlobe could convert to mat-format (figure

6.9). The steps I used are as follow:

1. Download OSGeo4W Network Installer (64 bit) (QGis) and install.

2. Download DEM maps: https://hoydedata.no/LaserInnsyn/, choose options: draw polygon, høydemodell, nasjonal høydemodell, laste ned DTM 50 datasett (50x50 meter pixel size), GeoTiff format, no compression method, coordinate system = as data set, file parts = as data set.

3. Using QGIS to convert from 33N coordinates to WGS 84, EPSG 4326: -raster-> projections-> warp(reproject) Coordinate reference system Source SRS = Generated CRS Target SRS = WGS84, EPSG: 4326

4. merging the parts of DEM GeoTiff given by 'kartverket': -raster-> miscellaneous-> Merge-> Find input files and create an output file.

5. Translate the output file from .tif to .asc format: Go to command window (write cmd in windows) and write: $gdal_translate - of AAIGrid - otInt16/path/"inputfile.tif"/path/"outputfile.asc"$.

6. Convert with mGlobe: Open the mGlobe window -> models -> DEM, choose asc-format as input and mat-format as output.

The DEM around Trysil observation station:

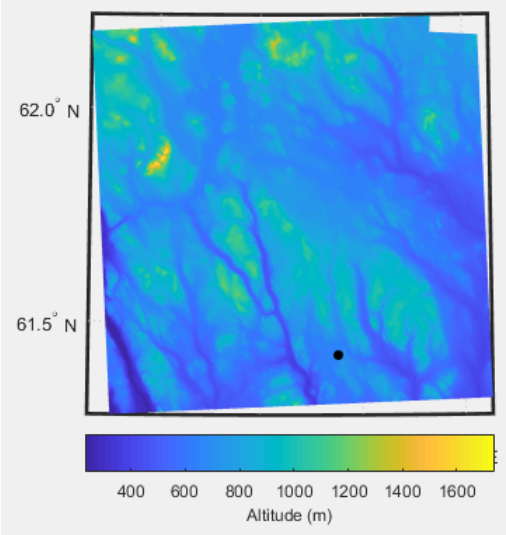

Figure 6.9: The DEM used for the LHM around Trysil observation station(marked)

Chapter 7

Computations, signals found, compare signals to absolute data

The gravity correction results for the five observation stations is presented and discussed in this chapter. The global effect from 0.05 spherical degrees from the observation point and outwards will be compared to the global effect outside of 0.1 and 1 degree. The local effect is computed with a higher resolution DEM inside of the 0.05 degree threshold. The GHM is tested with and without DEM and with ocean layer from mass excesses on and off. The nine different GHM will also be compared to each other and discussed. All the graphs are from the start of 2014 to the end of 2016 along the x-axis and gravity variation in μGal along the y-axis. The higher on the y-axis, the larger the hydrological correction is on absolute gravity. I scripted my own plotting function(Appendix, *plotting*) since the built in plot function in *mGlobe* could only include 5 graphs in one figure and did not include legends or axis-labels for the graphs. I have chosen to show the gravity correction of the hydrological models in the graphs. The absolute gravity is then absolute gravity observations plus the correction. In *mGlobe* the gravity effect of the

model or the effect minus the average effect for the model can be computed. To show the correction I have done, the effect is multiplied by -1. If the correction is smaller than 10% of the FG5 instrument precision (1-2 μGal), the impact of the correction is insignificant.

7.1 Comparing the impact of global and local hydrological models

The impact of GHMs and the LHM is analysed in this section. The gravitational impact from the local hydrological model (LHM) can be very different for each observation station because the topography and climate around the observation points is different. The impact of the attraction correction for GHM variations on gravity will not be as huge as the LHM variation wherever on earth the observation point is, since the effect diminishes with the distance as shown in chapter 2. The 9 GHMs for Trysil is shown in this figure:

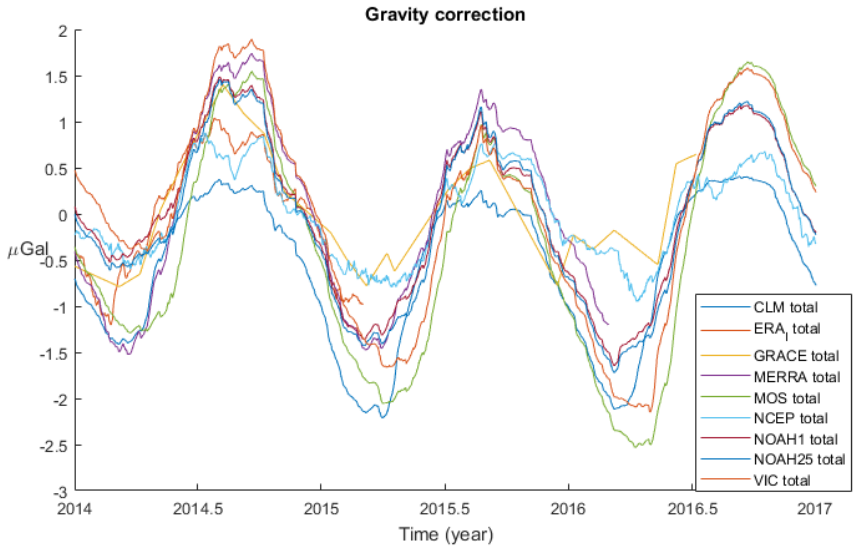

Figure 7.1: All the GHMs gravity correction with subtracted mean. Observation point: Trysil. GHM: All. Mass conservation: Ocean layer. DEM: on. Inner threshold: 0.05

In the figure below, the average of the NCEP and all the GLDAS GHMs variation are plotted together with the local hydrological variation for the Trysil observation station. ERAI, GRACE and MERRA GHMs did not have data for all 3 years, so those are excluded when computing the average global hydrological correction. The global and local DEM is used outside and inside of the 0.05 spherical degree distance respectively. Ocean layer from mass excesses is also used.

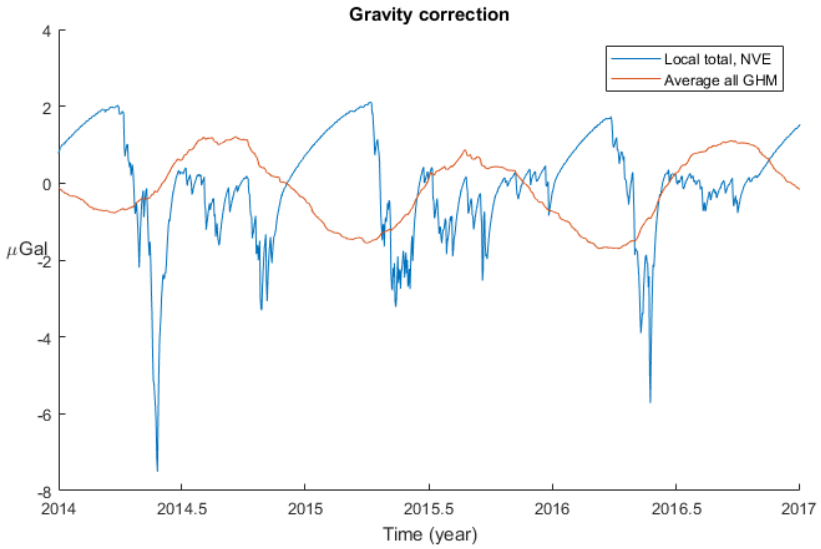

Figure 7.2: All the GHM together with the LHM in one plot, Trysil is the observation point. GHM: Average. Mass conservation: Ocean layer. Global and local DEM: on. Inner threshold: 0.05

The local variation in the groundwater fluctuates within a 10 μGal span, while the average of the GHMs have a variation of 3-4 μGal peak-to-peak. During the winter season, the local water table in Trysil declines, therefore the gravity effect of the groundwater also declines. This is described in the NVE groundwater description[NVE, 2015]. In the spring the snow is melting and the snow filtrates through the ground and raises the groundwater table.

In the PhD thesis Kristian Breili [Breili, 2009] wrote, the gravity effect of the ground water in Trysil is described on page 115. He calculated that the groundwater had a variation of 7 μGal from 2005 to 2008. Even though he computed for a different time period, it is interesting to compare the seasonal variations. The local effect in his thesis is defined within 200 m, and the regional effect from 200m to 200 km. The inner most zone 500 meters from the observation station the prism method is used. The prism method do not use a DEM, which means the water within 500 meters have a 10 meter lower height than the observation station. From 500m to 0.05

spherical degrees a high resolution DEM is used, and from 0.05 to 1 degree a rough DEM is used. Outside of 1 spherical degree from the observation point, no DEM is used. The total gravity correction is the sum of the GHM and the LHM shown in figure 7.3

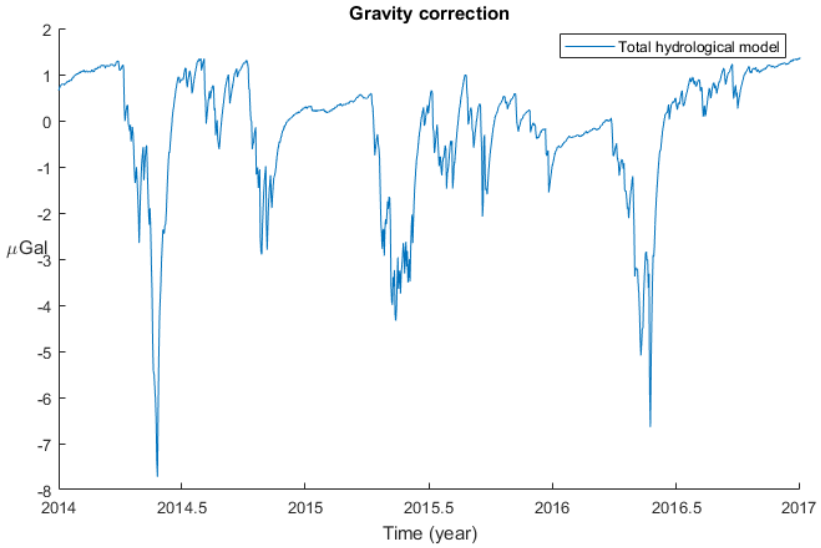

Figure 7.3: Total gravity correction between from 2014 to end of 2016, Observation point: Trysil. GHM: Average. Mass conservation: Ocean layer. Global and local DEM: on. Inner threshold: 0.05

The total gravity correction displayed for Trysil is lower than the local correction during the winter since the top of the curves are diminished when adding the global hydrological correction. This means that observation stations where the ground is freezing in the winter the local and global correction will counteract each other during the winter.

7.2 Comparing the gravity loading correction and gravity attraction correction for GHMs

The gravity loading correction and attraction correction is compared in this section. The diverse GHMs will have different gravity correction variation. The total gravity correction from the various GHM will probably have around the same part of percentage from the attraction effect and the loading effect.

When analysing the GHMs included here, I saw that they all consists of the same parts and the gravity effects are of the same order of magnitude for every GHM. Therefore I have chosen one GHM, the CLM, and investigated further. The total gravity correction variation computed from the CLM GHM at the observation point in Trysil is as follows

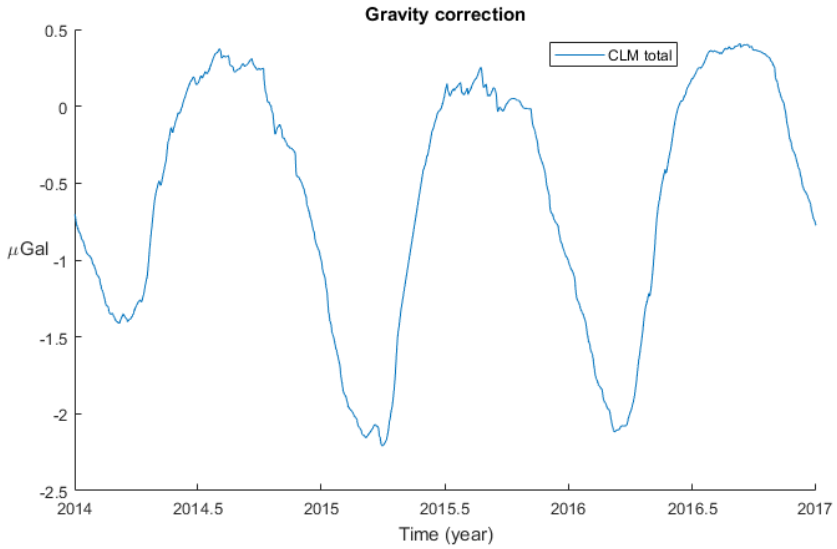

Figure 7.4: Total gravity correction for CLM. Observation point: Trysil. GHM: CLM. Mass conservation: Ocean layer. DEM: on. Inner threshold: 0.05

The seasonal cycle variation seems to vary a bit, every summer varies 0.1-0.2

μGal the years computed for Trysil This is insignificant when taking into the consideration of FG5 instrument precision. The seasonal cycle difference for the winter seems to vary a bit more, approximately -0.8 μGal from 2014 winter to 2015 winter. I have only analysed these 3 years, but the season to season hydrological cycle could be different in the past.

Looking closer at the CLM variation, the model varies within 2.5 μGal. The CLM is the sum of 4 types of gravity effects calculated for the GHM.

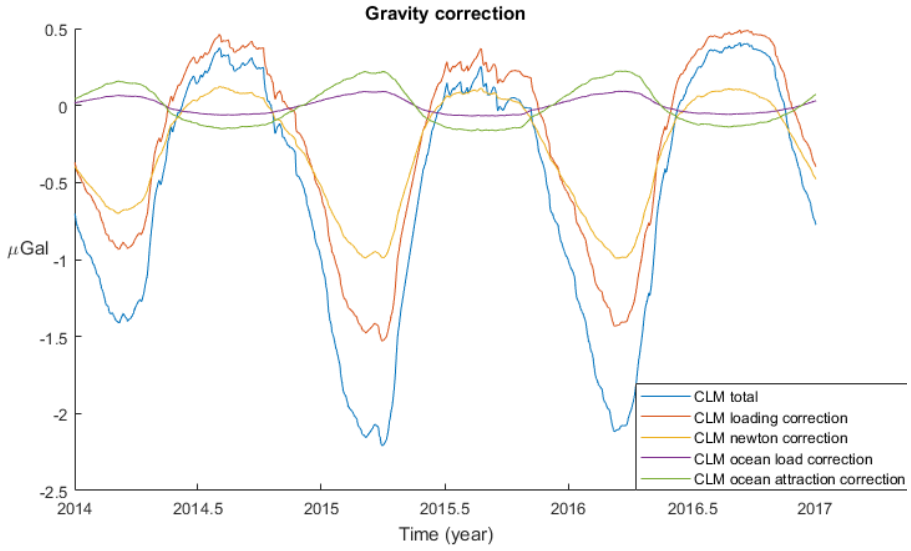

Figure 7.5: Total correction consists of 4 elements, the gravity surface (newton) attraction and loading correction, ocean loading and attraction correction from mass conservation. Observation point: Trysil. GHM: CLM. Mass conservation: Ocean layer. DEM: on. Inner threshold: 0.05

As seen above, the GHM CLM surface loading correction is varying from 0.5 μGal to -1.5 μGal and the surface attraction correction is varying from approximately 0.1 μGal to -1 μGal. Both corrections look similar to a sinus curve, they are also in the same phase. Peak-to-peak for the loading correction is nearly the double of the attraction correction. When comparing to the other GHMs calculated variations, it seems like the global loading

correction variates around twice as much as the global attraction correction.

The total correction is the sum of the loading and attraction correction plus the ocean loading correction and the ocean attraction correction. The ocean loading and ocean attraction correction is much smaller values and varies approximately from -0.1 to 0.1 and -0.2 to 0.2 μGal respectively. They have the same yearly frequency as the surface loading and attraction correction, but with half a year phase difference. That is because continental water storage needs to be taken out of the ocean and the surface to correct for the mass conservation.

The total gravity correction will change a bit when removing the mass conservation of the ocean layer, even though the effect is small.

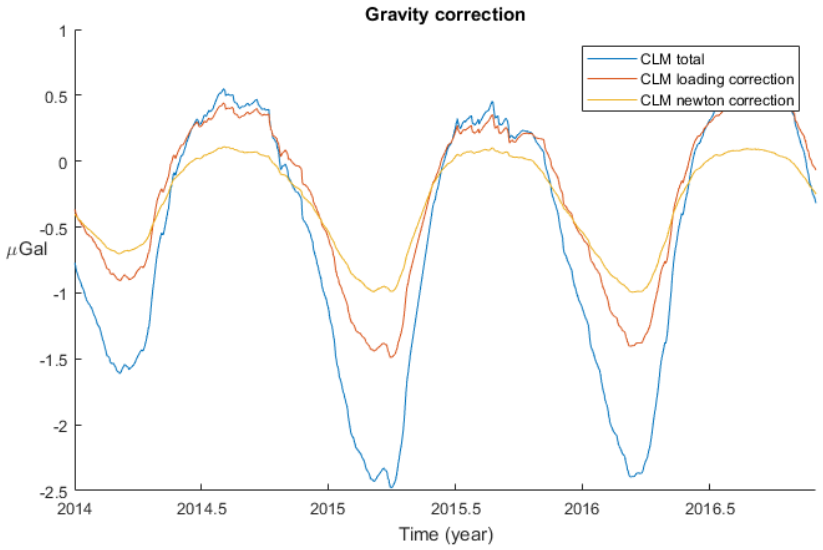

Figure 7.6: Gravity surface attraction and loading correction and the sum of them. Observation point: Trysil. GHM: CLM. Mass conservation: on. DEM: on. Inner threshold: 0.05

Without the mass conservation with ocean layer included, the total gravity correction have a larger variation from summer to winter, since the ocean

loading and attraction have a phase difference of half a year. The amplitude is now from 0.6 to -2.5 μGal (3.1 μGal difference), or approximately 0.3 μGal more from peak-to-peak than with ocean layer. The amplitude growth in percentage when the mass conservation is off will then be:

$$100\% * (3.1 - 2.8)/(2.8) = 10.7\%$$

When analysing data from the other observation stations and GHMs, they have a similar effect when turning off the mass conservation.

While the gravity loading and attraction correction for the GHMs have the same phase for Ås NMBU, Ringkollen, Trysil and Bodø, the Jondal 2 observation station is a special case. The gravity loading and attraction correction have a phase difference of half a year or 180 degrees (figure 7.7). (The gravity ocean loading and ocean attraction correction is still the same as in figure 7.5).

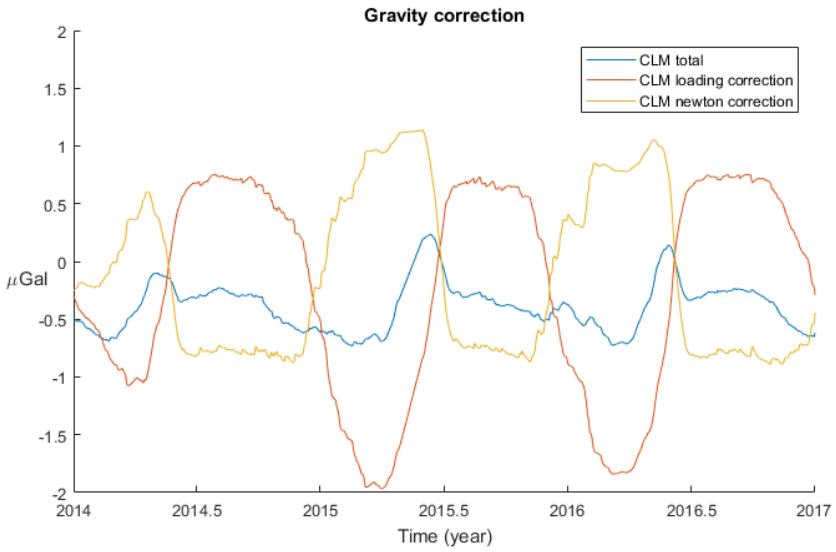

Figure 7.7: Gravity surface attraction and loading correction and the sum of them. Observation point: Jondal 2. GHM: CLM. Mass conservation: on. DEM: off. Inner threshold: 0.05

Jondal 2 have high mountains around it, so the hydrological elements are stored in the topography above the observation station. If there is a mass surplus (compared to average) than the loading has its maximum impact. This means, there are more hydrological masses around which will also have a peak effect on gravity. In this is the case, then the surplus of continental water pulls upwards, such that the gravitational effect is negative (acting against gravity) and thus opposed to the loading, which will contribute positively to gravity. This is not the case for the other 4 observation stations. With a height 0 and no topography from the DEM used, the CLM GHM looks like this for Jondal 2:

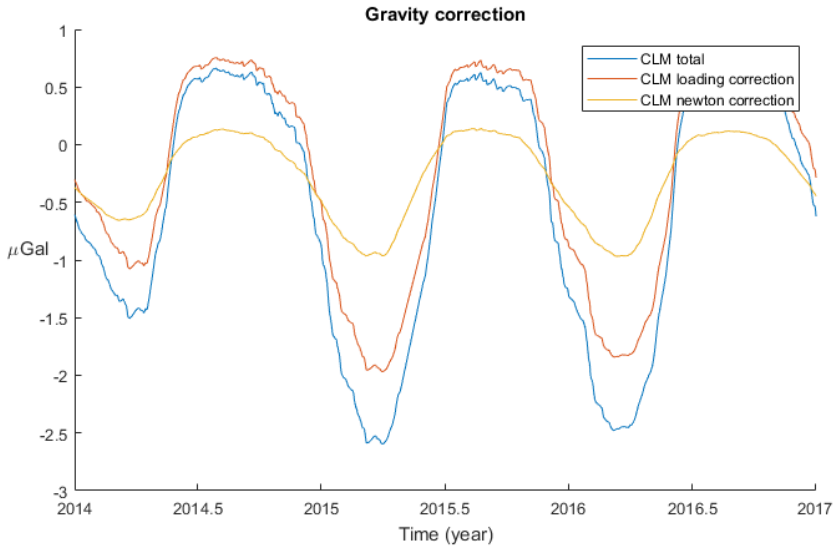

Figure 7.8: Gravity surface attraction and loading correction and the sum of them. Observation point: Jondal 2. GHM: CLM. Mass conservation: on. DEM: off. Inner threshold: 0.05

The topography is not accounted for in this figure, therefore the gravity loading and attraction have the same sign of attraction.

7.3 The impact of a DEM and inner threshold on GHM

A rough DEM around Norway(called global DEM in this thesis) as described in the last chapter is used to calculate the GHM variations, but the effect of the global DEM is minimal on hydrology. When the DEM is not used, the height of the observation station is put to zero in the *mGlobe* program. Figure 7.9 shows the difference between using a DEM and not using a DEM. When not using a DEM, the height is set to zero.

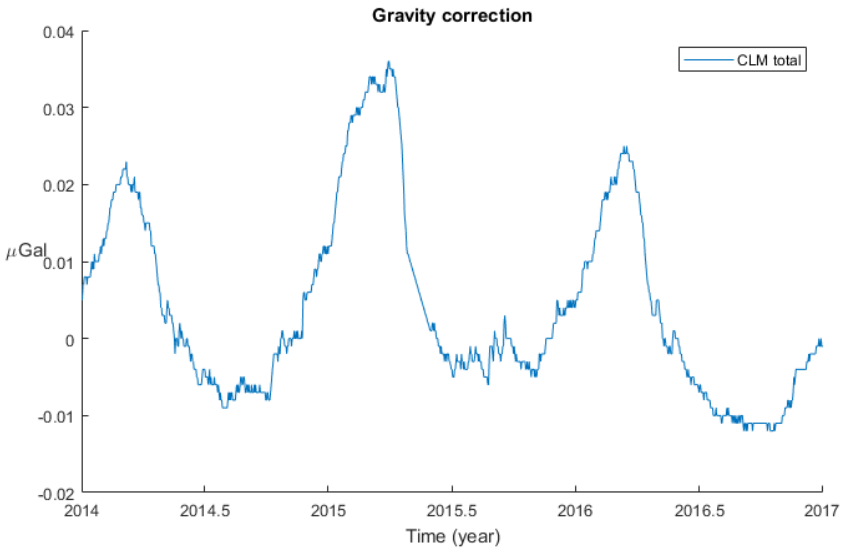

Figure 7.9: Total gravity correction, difference between using a global DEM and not using a DEM. Observation point: Trysil. GHM: CLM. Mass conservation: Ocean layer. DEM: on minus off. Inner threshold: 0.05

The effect of using a DEM is 0.05 μGal peak-to-peak, which is insignificant when using FG5 observations. This means a global DEM may not be needed when computing the GHM gravity correction for an observation.

The inner threshold of the GHMs can be chosen between every number

from 0.05 to 1 spherical degree in *mGlobe*. Mikolaj stated [Mikolaj2, 2016], page 13: "The calculation it self is divided into several zones depending on the spherical distance ψ between the mass and the measurement point. The closer to the measurement point, the higher is the degree of spatial discretization", end quote. The difference between using a inner threshold of 0.05 and 0.1 spherical degrees is shown in this figure:

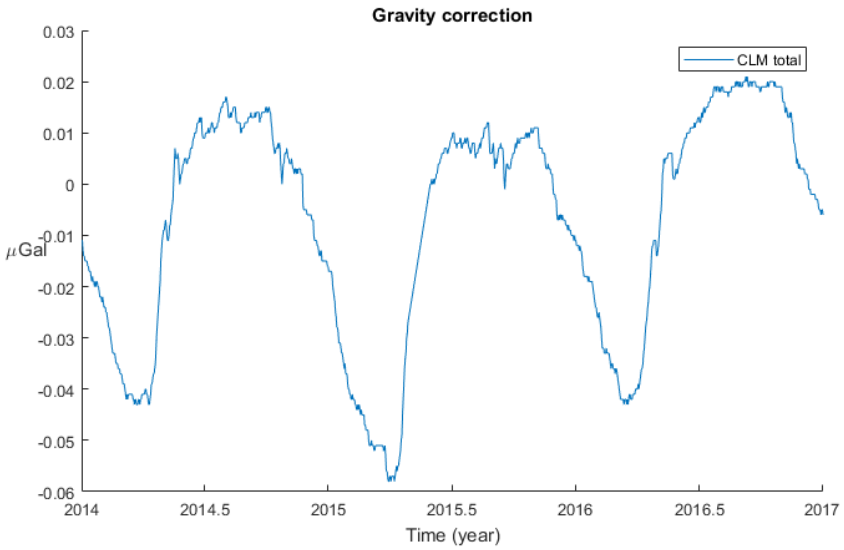

Figure 7.10: Gravity surface attraction and loading correction, ocean loading and attraction correction. Observation point: Trysil. GHM: CLM. Mass conservation: Ocean layer. DEM: on. Inner threshold: 0.05 minus 0.1 degree

The GHM variation between 0.05 and 0.1 degrees is 0.08 μGal and the impact of that "ring" is not significant. Comparing that to the difference between 0.05 degrees and 1 degree:

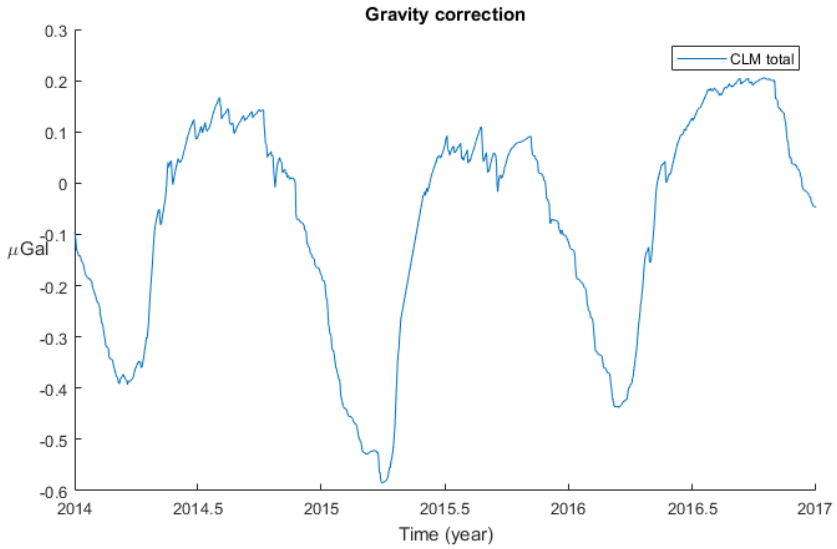

Figure 7.11: Gravity surface attraction and loading correction, ocean loading and attraction correction. Observation point: Trysil. GHM: CLM. Mass conservation: Ocean layer. DEM: on. Inner threshold: 0.05 minus 1 degree

The sum of the the rings with 0.05 degrees spherical distance from 0.05 to 1 degree is significant since the peak-to-peak correction is 0.8 μGal. Even though 0.8 μGal is less than the precision of the instrument, the impact of the inner threshold of the GHM has to be considered when computing the hydrological effect.

7.4 Comparing the hydrology variations at the different observation points

When looking at the local and global gravity corrections for the 5 different observation sites, it is shown that they fluctuate according to how close to the ocean they are, the topography around them, if there are frost or not in the ground during the winter and how rocky an area is. All figures in this section use the global DEM for the GHM and a high detailed DEM for the

LHM. The LHM is used from 0 to 0.05 spherical degrees and the GHMs are used from 0.05 degrees and outwards. Mass conservation is chosen as ocean layer. The local gravity correction for the observation sites over the 3 years are plotted:

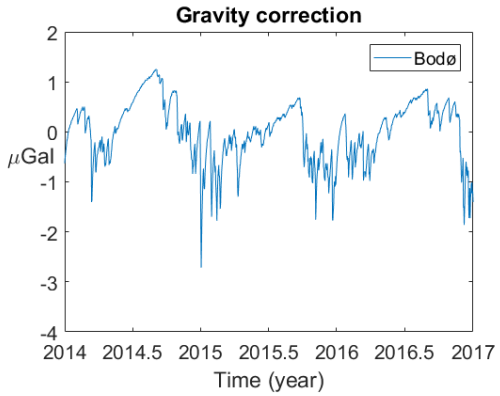

(a) Bodø

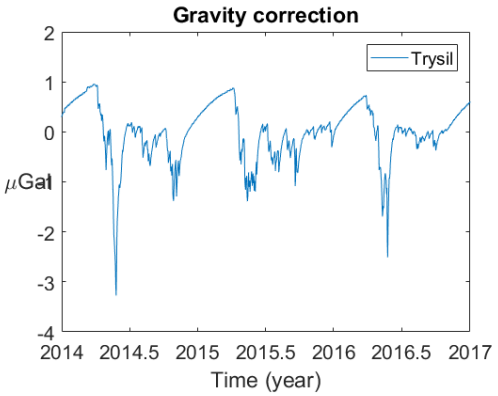

(b) Trysil

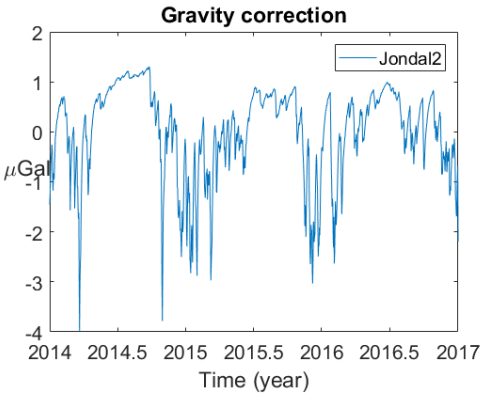

(c) Jondal 2

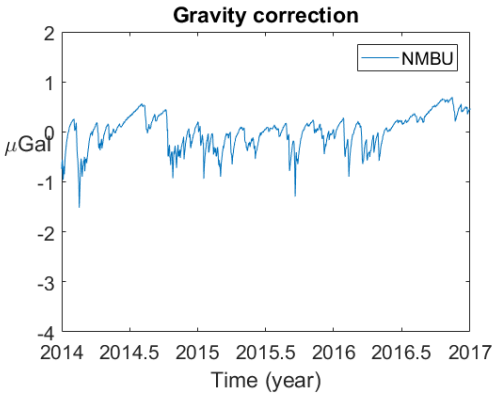

(d) Ås NMBU

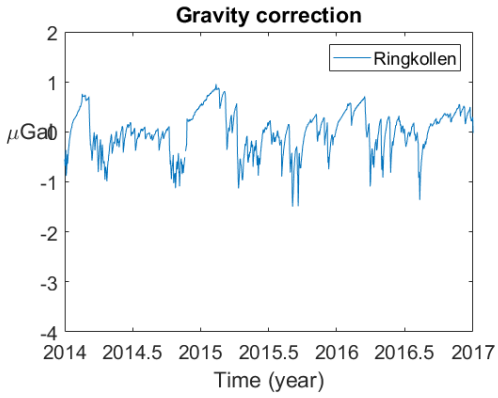

(e) Ringkollen

Figure 7.12: Local groundwater gravity correction variations for all the computed observation sites.

The groundwater gravity attraction correction for Bodø and Jondal is negative during the winter since there is rain in that period along the coast and the groundwater table rises. The groundwater table decreases during the summer in coastal areas until September when it starts to climb again[NVE, 2015]. In hilly and mountainous areas where the snow do not melt during the winter, the groundwater decreases and the gravity correction increases, as shown in the Trysil graph. In lowlands and areas which are not snow secure like Ringkollen and Ås, the groundwater fluctuates more randomly during the years.

The GHMs average gravity correction for the 5 sites is as follow

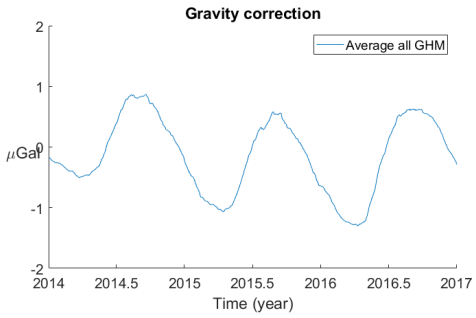

(a) Bodø

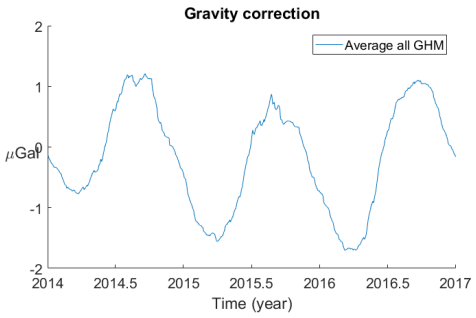

(b) Trysil

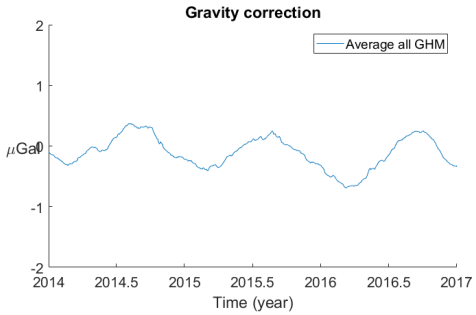

(c) Jondal 2

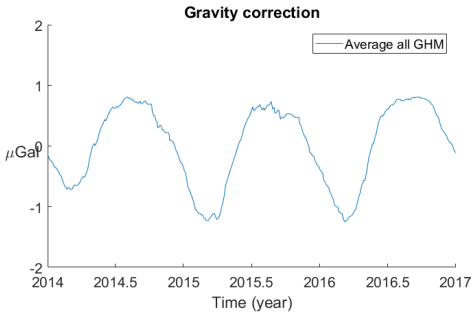

(d) Ås NMBU

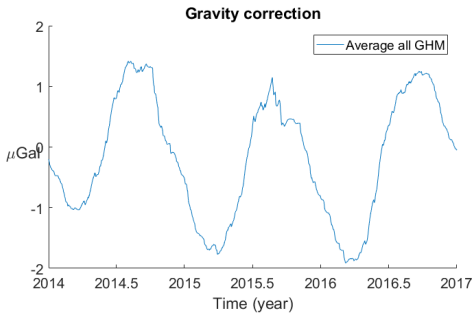

(e) Ringkollen

Figure 7.13: GHM gravity correction variations for all the computed observation sites.

The GHM correction for the different observation sites vary, the surface

loading and attraction for Jondal 2 station is contributing the opposite way when considering the gravity correction (as explained in section 7.2).

The sum of the local and global hydrological is plotted:

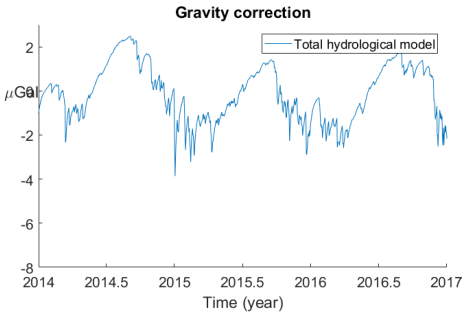

(a) Bodø

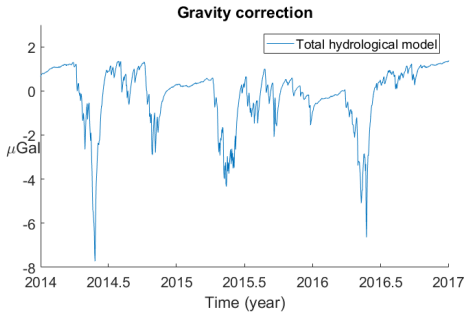

(b) Trysil

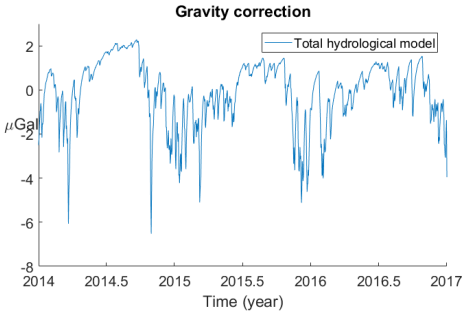

(c) Jondal 2

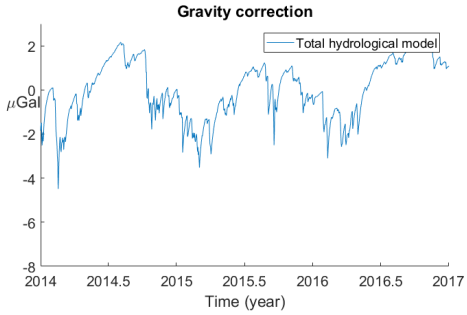

(d) Ås NMBU

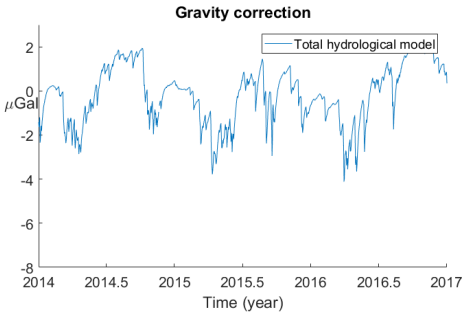

(e) Ringkollen

Figure 7.14: Total gravity correction variations for all the computed observation sites.

The gravity correction from the hydrological contribution is reflected in the local groundwater content and topography, the ocean loading and attraction effect, the continental loading and attraction effect. The local groundwater content have a bigger effect on the gravity and changes more rapidly than the contributions from the GHMs. These effects is easily detected with the superconducting and the absolute gravimeter.

Chapter 8

Summary and outlook

The Earth's gravity field consists of many elements of geophysical nature. Complex mathematical and empirical models tries to explain these constituents, but they are only approximations. One of these types of complex scientific models is the hydrological model.

Below follows a summary of what I have investigated and analysed in this thesis. Additionally, I will provide some final conclusions and further outlook.

In chapter 2, I explained physical geodesy; importance of the geoid and equipotential surfaces on the height systems, accordingly the gravity on the Earth is investigated. I explain how the instruments which are used to measure relative and absolute gravity works. The various hydrological models and their respective models are explained and listed. I have computed global and local hydrological contribution to the gravity with Matlab. I have analysed the results and discussed them. The results are compared to each other and the significance of the results regarding gravity instruments. The order of magnitude of the gravity correction elements and how they interact is discussed. The global hydrological models have a maximum correction of $\pm$ 2 μGal, where 60% is caused by the gravity loading correction and 40% by

the gravity attraction. For the local models, most of the gravity correction is coming from the attraction correction. The biggest peak-to-peak for the total local gravity correction is at the Jondal 2 station, which have 5.5 μGal difference. At the NMBU station the difference was the smallest of them all; only a variation of between 2 μGal during the 3 years (2014 to 2016). The total gravity correction have a variation of up to 10 μGal during a year at the Trysil observation station.

Together with hydrological models I have tried to explain some of the variations in the gravity, which improves the precision of measuring the gravity field around the Earth. The models which are used in this project fit our aim to understand the impact of the hydrological cycle as regards the gravity. The 1km resolution for the global DEM and 50 m resolution for the local DEM when regard the hydrological models 1 km is bad for superconducting fit with absolute gravity, which have 0.1 μGal precision. Especially since the inner most 500 meters is replaced with the prism method.

Further work would be to compare the gravity corrections directly with the absolute gravity data from the observation stations used in this thesis. Additionally, variations in the seasonal cycle, could be compared with Ophaug's data. Moreover, are there phase shift in the gravity corrections from the years he computed for? Has the maximum amplitude changed over the years [Ophaug et al., 2016]?

The groundwater is stored in the same height as the DEM, that means the depth of the groundwater table is not accounted for. If data for this can be retrieved with an even higher resolution than the NVE groundwater model, it will make a positive impact regarding the precision of gravity correction. Ice and snow cover is excluded from the computations, the impact of this act as a buffer for the precipitation. However, as the gravity observations are mainly done in the summer when the snow is melted, the gravity corrections in this thesis can be used for that period. Still, to compute a more accurate result, the snow contribution could be added to the continues gravity time series during the winter season.

Bibliography

[Breili, 2009] Breili, K., Investigations of surface loads of the Earth - geometrical deformations and gravity changes, Department of mathematical sciences and technology, Norwegian University of Life Sciences, Ås, Norway

[HBV model, 2015] Langsholt, E., Beldring, S., HBV-modellen, Norwegian Water Resources and Energy Directorate, URL = https://www.nve.no/hydrologi/analysemetoder-og-modeller/hbv-modellen/ (accesed 16.04.2017)

[Winter et al., 1998] Winter, T. C., Harvey, J. W., Franke, O. L., Alley, W. M., Ground Water and Surface Water, A Single Resource, U.S Department of the Interior, U.S Geological Survey, Denver, Colorado

[NVE, 2015] Norges vassdrag og energidirektorat, Grunnvann i Norge, 2015

[Forte, 2016] Forte, E., Introduction to geophysical methods, Universita Degli Studi Di Trieste, Naxos, Greece

[Rodell et al, 2004] Rodell, M. Houser, P.R., Jambor, U. ,Gottschalck, J., Mitchell, K., Meng, C.J., Arsenault, K., Cosgrove, B., Radakovich, J., Bosilovich, M., Entin, J.K., Walker ,J. P., Lohmann, D., Toll, D., 2004. The global land data assimilation system. Bull. Am. Meteorol. Soc. 85, 381–394

[van Westrum D., 2001] Derek van Westrum, FG5 Absolute Gravimeter, Micro-g LaCoste, 2001.

[Mikolaj, 2016] Mikolaj, M., mGlobe User Manual, GFZ German Research Centre for Geosciences, Section Hydrology, Potsdam, Germany

[Mikolaj, 2015] Mikolaj, M., Meurers, B., Mojzes, M., The reduction of hydrology-induced gravity variations at sites with insufficient hydrological instrumentation, GFZ German Research Centre for Geosciences, Section Hydrology, Potsdam, Germany

[Mikolaj2, 2016] Mikolaj, M., Modelling of global mass effects in hydrology, atmosphere and oceans on surface gravity, GFZ German Research Centre for Geosciences, Section Hydrology, Potsdam, Germany

[Reichle et al., 2011] Reichle, R. H., Koster, R. D., DeLannoy, G. J. M., Forman, B. A., Liu, Q., Mahanama, S. P. P., Touré, A., 2011. Assessment and enhancement of MERRA Land surface hydrology estimates. J. Clim. 24, 6322–6338

[Dee et al., 2011] Dee, D. P., Uppala, S. M., Simmons, A. J., Berrisford, P., Poli, P., Kobayashi, S., Andrae, U., Balmaseda, M. A., Balsamo ,G., Bauer, P., Bechtold, P., Beljaars, A. C. M., vandeBerg, L., Bidlot, J., Bormann, N., Delsol, C., Dragani, R., Fuentes,M., Geer,A.J., Haimberger, L., Healy, S. B., Hersbach, H., Holm, E.V., Isaksen, L., Källberg, P., Köhler, M., Matricardi, M., McNally, A. P., Monge-Sanz, B. M., Morcrette, J. J., Park, B. K., Peubey, C., deRosnay, P., Tavolato, C., Thépaut, J. N., Vitart, F., 2011. The ERA-Interim reanalysis: configuration and performance of the data assimilation system. Q. J. R. Meteorol. Soc.137, 553–597.

[Skaar K., 2015] Skaar, K., Cryospheric Mass Variations from GRACE, Department of mathematical sciences and technology, Norwegian University of Life Sciences, 2015

[Timmen L., 2010] Absolute and relative gravimetry. in: Xu (ed) Science of Geodesy - 1: Advances and future directions.

[Kalnay et al., 1996] Kalnay, E., Kanamitsu, M., Kistler, R., Collins, W., Deaven, D., Gandin, L., Iredell, M., Saha, S., White, G., Woollen, J., Zhu, Y., Leetmaa, A., Reynolds, R., Chelliah, M., Ebisuzaki, W., Higgins, W., Janowiak, J., Mo, K. C., Ropelewski, C., Wang, J., Jenne, R., Joseph, D., 1996. The NCEP/NCAR40-year reanalysis project. Bull. Am. Me- teorol. Soc. 77, 437–471.

[Landerer et al., 2012] Landerer, F. W., Swenson, S. C.,2012. Accuracy of scaled GRACE terrestrial water storage estimates. WaterResour. Res. 48, W04531.

[Fang et al., 2009] Hongliang Fang, Hiroko K. Beaudoing, Matthew Rodell, William L. Teng, Bruce E. Vollmer, Goddard Earth Sciences Data and Information Services Center, Code 610.2, Goddard Space Flight Center, NASA, Greenbelt, MD 20771, Hydrological Sciences Branch, Code 614.3, Goddard Space Flight Center, NASA, Greenbelt, MD 20771 3 Wyle Information Systems 1651 Old Meadow Road, McLean, VA 22102 4 Earth System Science Interdisciplinary Center, University of Maryland, College Park, MD 20742

[Gayathri et al., 2015] Gayathri K. Devi, Ganasri B. P, Dwarakish G. S. A Review on Hydrological Models, Department of Applied Mechanics and Hydraulics, National Institute of Technology Karnataka, Surathkal, 575 025, Mangalore, Karnataka, India

[Gjevestad, 2016] Gjevestad J. G., Introduction to physical geodesy, Department of mathematical sciences and technology, Norwegian University of Life Sciences, 2016

[Hoffmann-Wellenhoff et al., 2005] Hofmann-Wellenhoff, B., Moritz, H., Physical Geodesy, Institut für Navigation und Satellitengeodäsie, Technische Universität Graz, Graz, Austria, Springer

[Cushman-Roisin et al., 2009] Cushman-Roisin, B., Beckers, J. M., Introduction to Geophysical Fluids Dynamics, Academic Press, 2009

[Yilmaz, 2008] Yilmaz, N., Comparison of different height systems, Geospatial Information Science, 209-214, 2008

[Yi et al., 2015] Yi, S., Sun, W., Characteristics of gravity signal and loading effect in China, Laboratory of Computational Geodynamics, University of Chinese Academy of Sciences, Beijing 100049, China

[Amante et al., 2009] Amante, C., Eakins, B.W., ETOPO1 1 Arc-Minute Global Relief Model: Procedures, Data Sources and Analysis. NOAA Technical Memorandum NESDIS NGDC-24. National Geophysical Data Center, NOAA. doi:10.7289/V5C8276M (accessed 17.04.2017).

[Mikolaj, 2016] Mikolaj, M., mGlobe User Manual, GFZ German Research Centre for Geosciences, Potsdam, Germany

[Pagiatakis. 1998] Pagiatakis, S. D., Ocean Tide Loading on a self-gravitating, compressible, layered, viscoelastic and rotating earth with solid inner core and fluid outer core, Department of Surveying Engineering, University of New Brunswick, Frediction, N.B, Canada

[Gerlach, 2016] Gerlach, C., Lecture gravimetry 2016, Bavarian Academy of Sciences and Humanities, Munich and Department of Mathematical Sciences and Technology, Norwegian University of Life Sciences, Ås.

[Goodkind, 1999] Goodkind, J. M., The superconducting gravimeter, Department of physics , University of California, San Diego, La Jolla, California

[LaCoste, 2004] Lacoste & Romberg Instruction Manual Model G & D Gravity Meters, Austin, Texas 78758 U.S.A, Copyright @2004 LaCoste & Romberg

[Tsoulis, 1999] Tsoulis, D., Analytical and numerical methods in gravity field

modelling of ideal and real masses, Verlag der Bayerischen Akademie der Wissenschaften, München, Germany

[Farrell, 1972] Farrell, W. E., Deformation of the Earth by Surface Loads, Cooperative Institute for Research in Environmental Sciences, University of Colorado and National Oceanic and Atmospheric Administration, Boulder, Colorado

[NCEP Reanalysis, 2017] The Climate Data Guide: NCEP Reanalysis (R2), National Center for Atmospheric Research Staff(Eds). https://climatedataguide.ucar.edu/climate-data/ncep-reanalysis-r2 (accessed 25.03.2017)

[Ophaug et al., 2016] Ophaug, V., Breili, K., Gerlach, C., Gjevestad, J. G. O., Lysaker, D. I., Omang, O. C. D., Pettersen, B. R., Absolute gravity observation in Norway (1993-2014) for glacial isostatic adjustment studies: The influence of gravitational loading effects on secular gravity trends, Department of Mathematical Sciences and Technology, Norwegian University of Life Sciences, Ås, Norway, Geodetic Institute, Norwegian Mapping Authority, Hønefoss, Norway, Commision of Geodesy and Glaciology, Bavarian Academy of Sciences and Humanities, Munich, Germany

[Helland, 2014] Helland, A., Observation of Gravity Field Variations from Ground and Satellite Data, Norwegian University of Life Sciences, Ås, Norway

Appendix

compute the the gravity loading effect of 1 kg

```
%calculate the gravity loading effect of 1 kg 1 degree away
%L = importdata('mGlobe_DATA_dgE_Hydro.txt');
%L = importdata('listlovenumbers.txt');
L = importdata('LDcoe.txt');
m = 0;
n = 10000;
g = 9.81;
mod = 0;
M = 5.972*10^24;
psi = 1;
%f=pnm(n,m,psi,mod);
R = 6371000;

gL = 0;
%Define the sample points, n, and corresponding sample ...
    values, h, l, n.
% n = L(:,1);
% h = -L(:,2);
% l = L(:,3)./n;
% k = -L(:,4)./n;
n = L(:,1);
h = L(:,2);
l = L(:,4)./n;
k = L(:,6)./n;
```

```
%Define the query points to be a finer sampling over the ...
    range of n.

xq = 1:10000;
%Interpolate the function at the query points and plot the ...
    result.
nn = interp1(n,n,xq,'pchip');
ln = interp1(n,l,xq,'pchip');
hn = interp1(n,h,xq,'pchip');
kn = interp1(n,k,xq,'pchip');
% nn = interp1(n,n,xq);
% ln = pchip(n,l,xq);
% hn = pchip(n,h,xq);
% kn = pchip(n,k,xq);
figure
% plot(n,h,'o',nn,hn,':.');
%plot(n,l,'o',nn,ln,':.');
plot(n,k,'o',nn,kn,':.');
xlim([1 10000]);
title('love Load number');
temp = 0;
% hold on

% hold on
%
for n = 1:10000
        gL = gL + ...
            (-g/M)*(2*hn(n)-(n+1)*kn(n))*pnm(n,m,psi,mod);
end
%gL1mm39000 m^2
%lovenumbers ocean loading gL, n = spatial discretization

% gLv = 0;
% for n = 1:10000
%         gLv = gLv + R/M*hn(n)*pnm(n,m,psi,mod);
% end
```

load Love numbers

n	$-h_n$	nl_n	$-nk_n$
1	0.290	0.113	0
2	1.001	0.059	0.615
3	1.052	0.223	0.585
4	1.053	0.247	0.528
5	1.088	0.243	0.516
6	1.147	0.245	0.535
8	1.291	0.269	0.604
10	1.433	0.303	0.682
18	1.893	0.452	0.952
32	2.379	0.680	1.240
56	2.753	0.878	1.402
100	3.058	0.973	1.461
180	3.474	1.023	1.591
325	4.107	1.212	1.928
550	4.629	1.460	2.249
1000	4.906	1.623	2.431
1800	4.953	1.656	2.465
3000	4.954	1.657	2.468
10000	4.956	1.657	2.469
∞	5.005	1.637	2.482

Table 8.1: Load love numbers

Norges miljø- og biovitenskapelig universitet
Noregs miljø- og biovitskapelege universitet
Norwegian University of Life Sciences

Postboks 5003
NO-1432 Ås
Norway